Rapid Degradation of the Human ACE2 Receptor Upon Binding and Internalization of SARS-Cov-2-Spike-RBD Protein

Paul Feinstein[1, 2*]

[1]*Department of Biological Sciences, Hunter College, City University of New York, New York, NY 10065*
[2] *The Graduate Center Programs in Biochemistry, Biology and CUNY Neuroscience Collaborative, 365 5th Ave, New York, NY 10016*

*Corresponding author email: Feinstein@genectr.hunter.cuny.edu

[*]Correspondence:
Paul Feinstein
695 Park Avenue
904 North Building
Department of Biology
New York, NY 10065
Feinstein@genectr.hunter.cuny.edu

Running Title: Mitigation of SARS2 binding to ACE2 part I
Conflict of interest: The author declares that no competing interests exist.
Keywords: SARS-CoV-2; Spike protein; RBD, hACE2, Omicron variant, Xbb.1.5 variant, NL63, ACE2 downregulation

Contributions
P.F. conceived the project. P.F. designed the experiments. P.F. performed all experiments. P.F. analyzed the data. P.F. wrote the manuscript.

Abstract:

It is widely accepted that the SARS-CoV-2 betacoronavirus infects humans through binding the human Angiotensin Receptor 2 (ACE2) that lines the nasal cavity and lungs, followed by import into a cell utilizing the Transmembrane Protease, Serine 2 (TMPRSS2) cofactor. ACE2 binding is mediated by an approximately 200-residue portion of the SARS-CoV-2 extracellular spike protein, the receptor binding domain (RBD). Robust interactions are shown using a novel cell-based assay between an RBD membrane tethered-GFP fusion protein and the membrane bound ACE2-Cherry fusion protein. Several observations were not predicted including, quick and sustained interactions leading to internalization of RBD fusion protein into the ACE2 cells and rapid downregulation of the ACE2-Cherry fluorescence. Targeted mutation in the RBD disulfide Loop 4 led to a loss of internalization for several variants tested. However, a secreted RBD did not cause ACE2 downregulation of ACE2-Cherry fluorescence. Thus, the membrane associated form of RBD found on the viral coat may have long-term system wide consequences on ACE2 expressing cells.

Introduction:

The COVID-19 worldwide pandemic continues to produce widespread illness and death. The causative agent of this disease is the betacoronavirus SARS-CoV-2 (SARS2), which is similar the SARS1 virus that had a limited outbreak between 2002-2003 (1). The SARS1 infectivity was cut short by lockdowns, but was followed by a second betacoronavirus, MERS in 2012, which continues to infect individuals (2). Vaccines against SARS2 are reducing the death caused by the proliferation of viral particles (3-5). But vaccinations tend not to halt the transmission of viral particles, which occurs in just days after infection prior to the rise in immune response (6). In addition, the mutation rate of SARS2 is unyielding and we are now faced with the prospect of infections by novel variants for the foreseeable future. It is critical that the medical industry find viral transmission mitigation strategies (7-9). While masks form a reasonable barrier to SARS2 infectivity, societies have not embraced this as a long-term solution to mitigating infections.

How do SARS1 and SARS2 infections occur? It has been shown that the trimeric coat protein S1 for both viruses latch onto a cell via binding to a multimeric human Angiotensin-Converting Enzyme 2 protein, ACE2, that resides in the plasma membrane. ACE2 provides 740 amino terminal (Nt) residues in the extracellular space, whilst only a short 40 residue carboxy terminus (Ct) extends cytosolically (10-12). Once ACE2 is bound by S1, the Transmembrane Protease, serine 2**,** TMPRSS2 protein cofactor is believed to catalyze the endocytosis of the virus into the cell. Mitigating either binding of ACE2, functionality of TMPRSS2 (7, 8) or endocytosis could prove an effective means of suppressing disease onset.

ACE2 is well expressed in the cilia or microvilli throughout epithelial cells from the nose to the lungs. In the olfactory epithelium ACE2 is not expressed by olfactory sensory neurons (OSN) but robustly expressed on the intertwined supporting sustentacular cells (SUS) as well as Bowman's glands (13, 14). The nasal infection leads to a down-regulation of OSN produced odorant receptor (OR) signal transduction components (15). It is not completely understood how SUS cell infection by SARS2 contributes to anosmia (6). In our pursuit of studying odorant receptor protein trafficking to the plasma membrane, we have fused it and other G-protein Coupled Receptors to GFP and expressed them in an olfactory placodal cell line (OP6) with robust filopodia (16-18). Here we have repurposed the trafficking assay to study the molecular details of how the plasma membrane localize S1 Spike protein interacts with the ACE2 receptor.

Cellular entry for SARS2 is initiated by the 769 residue S1 subunit of the Spike protein. Detailed analysis of the SARS1-ACE2 binding subregion led to the identification of residues 333-529 as the receptor binding domain, RBD for SARS2 (19). This 197-residue region recognizes three domains within the first 357 residues of the ACE2 receptor. By contrast angiotensin II binds a different portion of ACE2 (20). The sufficiency of the RBD was shown in binding studies using a soluble form of ACE2, sACE2, which bound RBD in the micromolar EC50 range and to a dimeric ACE2 protein in the nanomolar EC50 range (21). The ACE2 protein traffics to the plasma membrane with a signal peptide that is cleaved resulting in the mature protein, residues 19-805. The RBD region binds to sixteen ACE2 residues distributed within its amino terminal (Nt) 19-83 residues, as well as another five residues within an internal region containing residues 330, 353-357. These interaction and crystallographic studies of SARS1 and SARS2 lay the foundation of this current work.

Here the RBD domain and full-length ACE2 proteins are linked to different fluorescent proteins to determine if they could interact. Initially, the Type I transmembrane ACE2 protein was fused with mCherry at its intracellular Carboxy terminus (Ct), whereas the 197-residue SARS2 RBD was fused to a secretion signal peptide along with either the Nt of single transmembrane (TM) domain protein or at the Nt of the 7-TM domain β2AR, both with GFP at their intracellular Ct.

This in vitro assay allowed us to observe fast and viral-free SARS2-RBD protein binding to ACE2 in cells, which mimic some of the binding and internalization properties of the pseudotype virus infection of ACE2 expressing cells: 1) rapid (a few minutes) and sustained binding between SARS2-RBD protein and ACE2; 2) a Spike S2 subunit independent uptake of a membrane bound RBD from one cell by other cells expressing ACE2; and 3) a down regulation of ACE2 protein upon binding to RBD suggesting an unsuspected effect on ACE2 accessibility for binding of additional viral particles. This novel in vitro assay provides the basis to identify the critical amino acid sequences involved in binding of SARS2-RBD to ACE2 and its internalization analogous to pseudotype viruses, which provide data on viral replication as a surrogate for RBD binding and viral membrane internalization by ACE2 expressing cells.

A multitude of generated mutations in conserved residues, despite being predicted to have important roles in binding from crystal structures, do not abrogate SARS2-RBD binding to ACE2 revealing the distributed nature of interactions. One critical residue that did not affect plasma membrane trafficking of the protein, Y489A, nearly abolished the RBD-ACE2 interactions. This residue juxtaposes C488 that is critical for disulfide Loop 4 formation (C480-C488). A debilitating C480A, C488A SARS2-RBD double mutant suggests that disruption of disulfide bridges would abolish binding to ACE2. RBD-ACE2 binding deficits were recapitulated in our assay using the disulfide reducing agent dithiothreitol (DTT) analogous to what has been demonstrated with pseudotype viruses. NL63-RBD contains three potential disulfide bonds with one cysteine residue common to SARS2 disulfide Loop 4 and containing three other homologous residues. Again, DTT blocked NL63-RBD binding to ACE2 as well. It is plausible that these or other volatile disulfide reducing agents could mitigate viral infections. Finally, the ability for RBD domains alone to affect ACE2 protein suggests that vaccines containing “binding competent” RBD domains may alter in vivo ACE2 protein levels and lead to adverse reactions. We speculate that vaccines with mutation(s) in RBD that cannot bind to ACE2 may lead to fewer side effects. Finally, some of the Long-COVID symptoms may be a result of sustained ACE2 down-regulation(22).

Results:

The RBD→ACE2 cell-based binding assay

The SARS-CoV-2 (SARS2) betacoronavirus infects cells via its cell surface protein, Spike S1. Internalization of the SARS2 virus is mediated by the Spike S1 binding partner, the Angiotensin 2 Converting Enzyme (ACE2) as well as a cofactor the Transmembrane Protease, Serine 2**,** TMPRSS2 protein, which cleaves the Spike protein revealing the S2 fusion protein. There have been many strategies to characterize the molecular interactions between the Spike S1 protein and its ACE2 receptor. Here we set up an in vitro cell interaction assay based on the experiments by Chan et al. (21), which measured the binding of a secreted (s) S1 subdomain-the receptor binding domain (RBD) fused to sfGFP fusion protein to various mutants of hACE2 expressed in heterologous cells (21). Using this information, we set up an in vitro expression assay to block these protein interactions **(Figure 1A).**

G-Protein Coupled Receptor (GPCR) trafficking to the plasma membrane (PM) has been studied by my lab for the last decade using an in vitro expression system where we transiently transfect GPCRs fused to fluorescent proteins into an olfactory neuronal cell line (OP6) that is rich in filopodia extensions (16-18). We previously showed that the presence of fluorescence in the filopodia accurately correlated with PM expression (16-18). OP6 cells are grown at 33°C, which is coincidently similar to the temperature at which the nasal epithelium would be infected by SARS2 in ambient air (23). We co-opted our expression system to study RBD and ACE2 interactions in vitro. Analysis was initiated with a mCherry fusion to the carboxy terminus (Ct) of human ACE2 and sfGFP fused to the Ct of the aforementioned secreted RBD. Filopodial expression of ACE2-Cherry **(Figure 1B-D and F).** In contrast, the secreted form of sRBD-sfGFP (s = hemagglutinin-cleavable signal) was detected only within the cell (not shown). When separate transfections were co-plated and cultured overnight, on occasion an ACE2-Cherry expressing cell could be seen with green particles suggesting uptake of secreted sRBD-sfGFP protein (not shown); The membrane of the ACE2-Cherry cells was not labeled with sRBD-sfGFP. These initial studies show that membrane secretion of sRBD-sfGFP may not be occurring.

In previous studies of GPCR tagging, the nicotinic receptor α7 subunit (nrα7) signal peptide (n) was shown to be effective in targeting a functional GFP added to extracellular portion of a GPCR (nGFP-GPCR) (24, 25). Thus, we tested the nrα7 signal sequence along with RBD to create nRBD-GFP and Delta-nRBD-GFP (delta SARS2 variant). Again, no membrane GFP fluorescence could be observed on ACE2-Cherry expressing cells. But it appeared that there may be some granules of GFP fluorescence within ACE2-Cherry cells after 12-18hr incubation. The interpretation of these result was either the sRBD-sfGFP or nRBD-GFP proteins were not secreted or if they were secreted, then perhaps they were rapidly internalized and degraded by the ACE2-Cherry expressing cells. Overall, these results suggested a reconsideration of this first approach.

The ACE2-Cherry fusion was successfully expressed at the PM but was unsuccessful at visualizing any GFP particle bound to ACE2-Cherry cells. Instead of secreting the RBD protein,

the nrα7-SARS2-RBD (nRBD) was tethered to the extracellular portion of the single transmembrane domain (TM1) of the mouse β2AR (the first 60 residues) that is also Ct fused to GFP. This generated nRBD-TM1- GFP and a control vector nTM1-GFP. Both fusions were expressed in cells and respectively co-cultured with ACE2-Cherry expressing cells. As expected nTM1-GFP trafficked to the PM but did not interact or transfer any fluorescence to the ACE2 expressing cells **(Figure 1B).** In contrast, the nRBD-TM1-GFP fluorescence was found on the tips of the filopodia expressing ACE2-Cherry **(Figure 1C and inset)**; It should be noted, ACE2-Cherry cells had well demarcated Cherry fluorescence in the filopodia and GFP expressing cells were not necessarily nearby. This result suggested that nRBD-TM1-GFP protein may have been secreted into the extracellular space. It should be noted that OP6 Cells do not express TMPRSS2 and no TMPRSS2 target sequences (Arg-Serine dimers) are found within this nRBD-TM1-GFP construct; Had there been any protein digestion, then no fluorescence could have been observed.

To fully secure the RBD domain to the PM, nRBD was tethered to the full-length, 7TM β2AR; these 7TM proteins cannot be secreted due to their seven hydrophobic domains. Transfection and co-plating and culturing of cells with the control nβ2AR-GFP and the control ACE2-Cherry (**Figure 1D**) or control β2AR-Cherry (**Figure 1E**), fusion proteins were found on the PM of the cells based on filopodial localization of the fluorescence; No transfer of fluorescence was observed between cells **(Figure 1D, 1E)** (16-18). When nRBD-β2AR-GFP expressing cells were co-cultured overnight with ACE2-Cherry expressing cells, robust cell-cell contacts and filopodial binding were observed **(Figure 1F and Inset)**. Moreover, ACE2-Cherry fluorescence was no longer well distributed in the cell and green-fluorescent particles could be observed within ACE2-Cherry cells as particulates. The Green fluorescent particles taken up by ACE2-Cherry expressing were indeed properly folded β2AR as they were able to bind a β2AR fluorescent antagonist (**Figure S1**, CellAura fluorescent $\beta_2$antagonist [(±)-propranolol]). We confirmed that Delta-nRBD-β2AR-GFP cells expressing the variant du jour, Delta (L452R, T478K)-RBD qualitatively interacted with ACE2-Cherry cells as did its parental "SARS2-RBD" form.

Our expertise in olfaction led us to surmise that there may be an odor that can interfere with SARS2-RBD binding to ACE2. With our protein interaction assay in hand, 36 concentrated odor mixtures from the kit "Le Nez Du Café (LNDV)"(26) were tested for their ability to antagonize RBD binding to ACE2. Only one of the mixtures at a 1:500 dilution, *medicinal*, appeared to visually reduce, but not eliminate binding; The degree of interaction could not be quantitated by microscopy. Had the odor completely blocked binding this would have been readily quantifiable. Thus, a quantification procedure to measure the extent of antagonism needed to be set up.

The RBD→ACE2 flow cytometry based binding assay

How strong is RBD-ACE2 cell-based binding of green fluorescence in or on red fluorescent cells? Would this be observed after trypsinization of co-cultures followed by single cell FACS analysis? The binding affinity of RBD to ACE2 has been previously calculated at nanomolar equilibrium rates (Kd)(1, 21). This was tested with overnight co-culture for various GFP fusions against ACE2-Cherry cells followed by trypsinization and FACs quantification of GFP positive cells, Cherry positive cells, and Cherry/GFP double positive cells. GFP fusions used were: nTM1, nRBD-TM1, nRBD-TM1 plus the odor mixture *medicinal*, β2AR, nRBD-β2AR, nRBD-

β2AR plus the odor mixture *medicinal*, Delta-nRBD-β2AR clone 1, Delta-nRBD-β2AR clone 2. Almost no Cherry/GFP double labeled cells were observed for the two controls nTM1 and β2AR **(Figure 2A).** But greater than 60-fold double labeled cells (56.53±6.05) were observed in the other six conditions **(Figure 2A).** These pilot experiments clearly demonstrated that RBD-ACE2 interactions could be quantified. Furthermore, quantification shows the odor *medicinal* **did not** mitigate binding. From this experiment, FACS-isolated Cherry cells, GFP cells, Cherry and GFP double labeled cells were obtained and microscopically analyzed each population: Green cells were revealed to largely contain GFP fluorescence and only rare fragments of ACE2-Cherry fluorescence could be observed, Cherry only cells did have some green fluorescence and the double labeled cells showed red cells with robust green fluorescence **(Figure 2B, 2B').** Flow cytometry experiments strongly argued that pieces of green-fluorescent membrane were being pulled from Delta-nRBD-β2AR-GFP expressing cells.

The RBD→ACE2 in situ single cell binding assay

The robustness of the RBD-ACE2 interaction suggested that the observe binding may be acute. To test this idea, trypsinized Delta-nRBD-β2AR-GFP expressing cells and ACE2-Cherry expressing cells were co-incubated at 37°C for 10 minutes; Indeed doublets of green and red fluorescent cells **(Figure 2C-C''')**. In addition, GFP/Cherry doublets showed aggregation of Cherry fluorescence at the edge of the cell were the green-fluorescent cells are making contact and weak Cherry fluorescent intensity throughout the remainder of the cell suggesting a rapid redistribution of the ACE2-Cherry protein.

Time course for acute RBD→ACE2 interactions

FACS analysis of double labeled cells proved to be a robust, quantifiable method to determine the degree of interactions between RBD expressing cells and ACE2 expressing cells. The acuteness of interactions between these cells, led us to set up a different assay where we would culture transfected cells overnight separately followed trypsinize "test construct" and plating them onto ACE2 expressing cells. Triplicate platings were performed for 10, 30, or 90 minutes (min) at 33°C. Following this incubation, cells on target plate were washed, trypsinized and quantified by flow cytometry analysis of single cells [*Dissociate-Plate-FACs (DPF) assay*]. As expected nRBD-β2AR expressing cells did not interact with ACE2 expressing cells at any timepoint **(Figure 2D).** But, for both nRBD-β2AR (SARS2-RBD) and Delta-nRBD-β2AR (Delta-RBD) expressing cells, 4.7 and 6.1-fold increases (± 1.5 and ±1.8, respectively) over background in double positive cells were observed in 10min, respectively; 13.4 and 13.1-fold increases (± 3.2 and ±2.7, respectively) in 30min, respectively; and 21.0 and 22.9-fold increases (± 2.8 and ±1.2, respectively) in 90min, respectively **(**Figure **2D).** Cell seeding is generally a slow process that takes hours, so the ~5-fold increase in double labeled cells was remarkable. When quantifying the ACE2-cherry fluorescent cells a noticeable decline in the number red cells at 10 min was observed reaching ~3-fold fewer numbers (a ~60% reduction ±5%) by the 90 min timepoint **(Figure 2D').** A 40%±16% reduction of ACE2 expression was observed in the pilot experiment **(Figure 2A')**. The rapid drop in ACE2 levels suggests either red cells have died in the 90 min period perhaps due to reorganization of membrane proteins or ACE2 protein is being rapidly degraded through RBD binding. Utilizing this new assay, it was confirmed that neither

secreted SARS2 nor Delta gave rise to GFP/Cherry double fluorescent cells **(Figure S2A)**, nor reductions in ACE2-Cherry expression **(Figure S2A')**. Several control experiments further validated the assay. Reducing the number of Delta-RBD cells added did not alter the affect, Delta-RBD cells did not interact with β2AR-Cherry cells, and most importantly the Delta-RBD cells did not cause the ACE2 expressing cells to be dislodged from the plate **(Figure S2A and S2A')** as GFP/Cherry doublets were not observed in the supernatant after a 90min co-culture. Overnight supernatant from Delta-RBD cells did not produce any GFP/Cherry doublets nor decreases in ACE2-Cherry fluorescence **(Figure S2B and S2B')**. A direct test of the secreted particle possibility utilized purified His tagged-RBD protein coupled to an anti-His-488 antibody and incubated for 90min with ACE2-Cherry expressing cells. No impact could be observed on the down regulation of ACE2-Cherry fluorescence despite the formation of antibody labeled ACE2 cells (**Figure S3A and S3A'**). In sum, there was no evidence of acute cell death nor secreted particles from the β2AR tethered RBD expressing cells.

Does cell adhesion cause down regulation of membrane proteins?

Thus far, the data show specificity between nRBD-β2AR-GFP expressing cells and ACE2-Cherry expressing cells. Yet, nonspecific interactions and ACE2-Cherry protein could be due to β2AR interaction or through the effects from an unidentified process of cell-cell adhesion. As a control Venus or Cherry fusions of the cell adhesion molecule Cadherin 2 (CDH2) were separately transfected and co-cultured overnight in OP6 cells producing robust cell-cell contacts compared to Delta-RBD and CDH2 **(Figure S2B)**. Interaction of CDH2 was observed as double fluorescent cells, however the red fluorescent of CHD2-Cherry was not decreased (**Figure S2B** and **S2B'**). To rule out the RBD-ACE2 interactions were phenocopying a cell adhesion phenomenon, a series of controls using ACE2-Cherry, β2AR-Cherry, CDH2-Cherry cells were set up that are co-incubated for 90min with β2AR-GFP, Delta-nRBD-β2AR-GFP, or CDH2-GFP cells, followed by FACS analysis; Only Delta-nRBD-β2AR-GFP and ACE2-Cherry cells led to double fluorescent cells and decreases in Cherry fluorescence of ACE2-Cherry (**Figures S2C, S2C'**). Double fluorescence cells derived by "cell adhesion" between ACE2-Cherry and Delta-RBD GFP cells was more impactful than that of CDH2-GFP + CDH2-Cherry cells in 90min co-cultures **(Figure S2C and S2C').** Here it can be firmly concluded that the observed cell dynamics are derived from RBD and ACE2 binding.

RBD→ACE2 membrane reorganization

We have previously shown that plasma membrane dynamics can be readily monitored by an array of palmitoylated fluorescent proteins [20-residue sequence (aka *gap*) from Zebrafish gap43] (16). To determine if the OP6 cells were undergoing general membrane changes from the RBD-ACE2 binding, ACE2-Cherry and gapTeal were cotransfected (Co-EP) and Delta-nRBD-β2AR-Venus cells were added and imaged after 30min **(Figure S4A-D''')**. Reorganization of the ACE2-Cherry fluorescence and Delta-nRBD- β2AR-Venus was readily observed, but not that of gapTeal **(Figure S4A, A')**. Quantification of fluorescent pixels showed co-accumulation of Venus and Cherry fluorescence at the plasma membrane, but not Teal **(Figure S4Bs)**. Unfortunately, quantification of these results by single cell FACS is not possible because Teal and Venus fluorescent proteins could not be separable by the available flow cytometry machines. But, FACS analysis of single cells can be performed with GFP, Cherry and

Farred fluorescent proteins. To circumvent this issue, the assay was reorganized. Now ACE2-GFP and gapFarred [codon optimized AFP (16)] were Co-EPd. Separately transfected Delta-nRBD-β2AR-Cherry, CDH2-Cherry or nβ2AR-Cherry were followed by trypsinization, co-plating and imaging within 30min over time **(Figure 3A-C'''**). Quantification of fluorescent pixels again showed co-accumulation of GFP and Cherry fluorescence at the plasma membrane, but not Farred **(Figure 3D)**. It is notable that the effects on membrane reorganization of ACE2 protein was independent of Ct fluorescent protein fusion: GFP fluorescence also appeared weaker suggesting it was being degraded. FACS analysis on single cells and confirmed the specific interaction of Delta-nRBD-β2AR-Cherry with ACE2-GFP showing 37.8 $\pm$6.1-fold more double positive cells than controls and a 47$\pm$4.3% reduction of ACE2-GFP fluorescence; Control proteins nβ2AR-Cherry and CDH2-Cherry did not associate with ACE2-GFP nor cause its down regulation **(Figure 3E and 3 E')**. Furthermore, gapFarred fluorescence was not altered in any of the conditions **(Figure 3E')**. The ACE2 internalization effects were even more profound after overnight co-plating **(Figures S4C-C''')** compared to controls **(Figures S4D-D''')**, which showed no internalization of ACE2. It should be noted that internalization of ACE2-Cherry did not lead to cell death. Finally, spinning disk imaging of the cell-based interactions with Delta-nRBD-β2AR-GFP and ACE2-Cherry cells were performed to show real-time dynamics; ACE2-Cherry reveal drastic reorganization, but not Delta-nRBD-β2AR-GFP cells within 10minutes of imaging **(Figures 3F, F' and Movies S1A-C)**. In sum, RBD specifically reorganizes and degrades ACE2-fluorescent proteins.

Meta-Analysis of 197 residue SARS2-RBD domain

Armed with the cell-based RBD-ACE2 interaction assay and are failure to find an odor mixture that could mitigate this protein-protein interaction, it became necessary for a first principles analysis of critical RBD binding residues; Knowing the residue(s) involved might lead to a more logical approach for odor identification. Residues 320-515 for the SARS1-RBD domain (74% identical to SARS2) were previously defined as essential for binding the ACE2 receptor were also compared **(Figure 4)** leading to the delineation of equivalent SARS2 residues (333-529). By reviewing the crystallographic data (1, 27), deep mutational screening (DMS) (21, 28), in silico predicted interactions (29) and the known properties of amino acids in proteins, a subset of residues that provide structural integrity and binding potential were identified.

DMS by two groups led to the identification of clones that can still bind the ACE2 receptor. Both groups produced very similar data, but one group also controlled for RBD stability revealing 29 residues that were not mutated in 70% of the clones and thus necessary for binding **(Figure 4, red highlights within SARS1-SARS2-RBD consensus sequence)**. Nine of these residues were retained in 90% of the DMS clones **(Figure 4, green lettering and green starred)** and would appear to be the most critical. From the 29 residues, only four Cys residues in disulfide bridges for Loop 2 and Loop 4 appear critical. Among the 29 red highlighted residues, only 10 distributed residues were residues not implicated in the folding of the RBD and thus candidates for ACE2 binding: F400, N422, Y423, S442, N487, Y489, Y495, F497, Q506, H511. As an apparent contradiction, residues predicted in silico to be critical for binding **(Figure 4, yellow highlights)** do not overlap any of the 29 relatively immutable residues from DMS clones: K417, F456, F486, Q493, Q498 (29). Only two residues (Y449, G496) are amongst the 29 residues that are subject to mutations in the various variants produced in first two years of the pandemic. The

greatest concentration of immutable residues lay between N487 and V511. Three residues described in the literature (Y449, N487, Y489, **Figure 4** purple highlighted) are predicted to affect binding when mutated (30). Finally, a set of three residues that overlap one end of disulfide Loop 4: N487, C488, and Y489 are well conserved in all known betacoronaviruses that bind the ACE2 receptor **(Figure S5)**. Overall, most interacting residues appear distributed, except for a stretch of residues between or near C480 and C488.

It is known that the alphacoronavirus H-CoV-NL63 (NL63-RBD) has a 135 residue RBD domain that also binds the ACE2 receptor. This domain has only ten residues conserved with SARS2-RBD, but four of them are colinear with the RBD disulfide Loop 4 region **(Figure S5 and S6; residues C-FPL)** (31). The NL63-RBD homology region is not among the residues predicted to interface with ACE2 **(Figure S6; RBM1-3)**, but it is interesting to note that the N578Y mutation that makes a five-residue match to the SARS2-disulfide Loop 4 region (CYFPL) increases its binding potential to ACE2 **(Figure S5)**(31). By contrast, the SARS2 homologue, RpYN06, is missing the region between C480 and C488 that comprises disulfide Loop 4 and fails to bind ACE2 **(Figure S7)**(32). Taken together, a strong argument can be made for critical ACE2 binding residues reside within the RBD-disulfide Loop 4 region that may include the pair of Cys residues.

RBD and disulfide Loop 4 region domain mutagenesis

An array of RBD variants and mutants including disulfide Loop 4 substitutions were tested to gain insight into the critical nature of RBD binding to the human ACE2 receptor. The SARS1, SARS2 and NL63 RBDs have been shown to bind the human ACE2 protein with Kds in the low nM range **(Figure S5)** (1, 31, 33). SARS2 variants have not been compared yet but are likely in the same range. One RBD, RaTG13 binds with a Kd in the μM range (1000-fold less) (**Figure S5)** (34). All four species and five SARS2 variants (Alpha, Delta, Delta-Plus, Omicron-BA.1, Omicron-BA.2) were tested **(Figures 4, 5, S8)**. No differences were observed in their ability bind and degrade ACE2, except for NL63, which produced fewer double positive cells but more severe degradation of ACE2 **(Figures 5A, 5A' and S8B')**. Alanine mutagenesis, converting all 3 high frequency mutants (>.03%) found in year 2020 and all 7 residues found in year 2020 and 2021. None of these mutations altered binding and degradation properties of SARS2-RBD **(Figure 5A, S8B, B'**). Next, seven RBD-ACE2 Predicted Binding Sites (P.B.S.) were converted into alanine. P.B.S. 7 Ala-RBD-β2AR-GFP trafficked to the plasma membrane but was not observed to bind ACE2-Cherry cells **(Figures 5A, 5B, S9A, S9A', S10B)**. This mutant was the first that completely blocked binding **(Figures 5)**, a 6.1±3.1-fold double positive rate compared to 3.0±1.8-fold in controls. One of the alanine substitutions was within the disulfide Loop 4, F486, might have been predicted might to be critical for RBD-ACE2 interactions. Indeed, the P.B.S. 6 Ala mutant with the A486F revertant could now bind to and degrade ACE2 **(Figures 5, S9B, S10C)**, 85.6±10-fold double positives, almost as well as SARS-RBD **(Figure S9C and S10A)** with 101.2±13.0-fold double positives. Other single reversions were not performed, but due to the distributed nature of binding; It is plausible that several might also rescue binding. It is likely that no one residue is critical for binding except F486, but this residue could be heavily mutated in the DMS experiments, suggesting that it does not form bonds that are necessary and sufficient of RBD binding. Taken together the vast number of residue differences between

RaTG13/SARS1 and SARS2 along with the alanine scanning mutations suggested that critical residues for binding are distributed throughout the RBD.

If RBD binding to ACE2 were distributed, then how are nanomolar Kds accomplished? Cross species sequence comparisons suggest disulfide Loop 4 may be key to nucleate ACE2 interactions. It is known that the tripeptide domains like Arg-Gly-Asp (RGD) may be small enough to achieve high affinity binding. Thus, a small motif within the RBD domain may be all that is necessary, but no such 100% conserved three residue region exists amongst RBD domains and mutants. Yet, the disulfide Loop 4 represented an interesting region as the disulfide bond itself may play a critical role in recognition of the ACE2 protein **(Figure 5B)**. In the context of SARS2-RBD, small regions between C480 and 488 were generated: SARS1 481-486 and RaTG13 483-486 substitutions as well as scanning alanine mutants for residues 486 through 492 **(Figures 5B and S8B**). Neither SARS1 and RaTG13 Loop 4 substitutions nor alanine mutants showed any differences in binding and internalization **(Figure 5)**. Based on the P.B.S. 6 Ala-RBD, the F486A alone might have disrupted binding, but it did not **(Figures 5)**, again pointing to the distributed nature of RBD binding to ACE2.

Alanine scanning of neighboring residues Y489, F490, P491, L492 and the Y449 residue predicted to be important for binding revealed several interesting aspects of RBD binding to ACE2. First, only Y489A was able to nearly abolish binding (14.7$\pm$6.6-fold double positives) and reduce degradation of ACE2 (30%$\pm$2.6%), while still being well expressed at the plasma membrane (**Figures 5, S8, S9, S10**). In contrast, the Y449A residue predicted to decrease binding of RBD had no effect. Second, C488A did not traffic well to the plasma membrane, but even when it did, binding and degradation was not readily observed. It seemed likely that teh C488A mutation that poorly traffics RBD to the plasma membrane may be due to the C480 residue forming a disulfide bond occurred with one of the other 6 Cys residues **(Figure 4).** To mirror the loss of both Cys residues found in RpYN06 **(Figure S7),** C480A, C488A-RBD was generated. This mutation traffics very well to the plasma membrane, on occasion binds ACE2-Cherry expressing cells, but does not become internalized **(Figures 5, S9)**. Third, neither N487A, F490A nor P491A affected plasma membrane trafficking nor binding/degradation properties of RBD. Finally, mutational analysis was expanded to the Omicron (OM).BA.1 variant for Y489A and P491A mutants. But neither mutant could traffic to the plasma membrane suggesting that OM.BA.1 had a different confirmational landscape to that of SARS2 or any previous variant **(Figures 5 and S10)**. Overall, the data strongly implicate the formation of the disulfide Loop 4 bond as a critical feature of RBD-ACE2 interactions.

Blocking RBD binding using a disulfide reducing agent

The analysis RBDs from NL63 and betacoronaviruses such as SARS1, SARS2 and its variants define a continuum of RBD residues necessary for allowing its internalization by ACE2. These data argue that it would be difficult to find an airborne molecule, which would specifically disrupt contacts between the changing landscape of RBD and ACE2 interactions. But the disulfide Loop 4 analysis suggested that critical Cysteine residues involved in disulfide bridges were common to all RBD domains could be a targeted to mitigate infection. That said, the volatile reducing agent Dithiothreitol (DTT) was able to disrupt SARS2 pseudotype virus infections on ACE2 expressing cells (35, 36). DTT has a strong characteristic odor with a modest

vapor pressure of 1.28 x10^{-4} mm Hg at 25C. A derivative of DTT, dithiobutylamine (DTBA) was identified in 2012 that had similar properties, but more resistant to changes in pKA and reduces disulfide bonds in small proteins more quickly (37). The RBD-ACE2 solution binding assay (**Figure 2C-C'''**) was utilized to assess GFP-Cherry in concentration series (0mM, 0.5mM, and 2mM) for DTT and DTBA. SARS2-RBD-β2AR-GFP or OM.BA.1-RBD-β2AR-GFP and ACE2-Cherry GFP/Cherry doublets were readily observed in the 0mM DTT and DTBA conditions for both SARS2 and OM.BA.1-RBD (**Figure 6A**). In the 2mM DTT condition it was difficult to find SARS2-RBD or OM.BA.1-RBD bound to ACE2 (Figure **6B and inset**). In contrast, RBD interactions were not observed in 2mM DTBA. The effect of reducing agents on SARS2 and OM.BA.1-RBDs in the solution binding assay mirrored what was already tested using pseudotype viruses, showing that binding assay strategy could be set up to screen for other volatile compounds for their ability to disrupt disulfide bonds. Finally, the NL63-RBD with a different set of disulfide bonds was quantified in the presence of 2mM DTT and 2mM DTBA in the plate binding assay with ACE2-Cherry. 2mM DTBA completely removed the ACE2-Cherry cells from the tissue culture plate, but the 2mM DTT did not, and these interactions were quantified by FACS; the 2mM DTT prevented double fluorescent cells from forming and prevented downregulation of ACE2-Cherry fluorescence (**Figure 6C and 6C'**). Thus, limited disruption of disulfide bonds in RBDs using a volatile disulfide reducing agents could provide a new strategy to mitigate viral infections.

Discussion:

Spike S1-RBD interactions with ACE2 are critical for cellular internalization

Respiratory coronaviruses like SARS1, SARS2 and NL63 utilize their spike protein to bind to the human ACE2 receptor on the surface of cells that line the respiratory epithelium. Mapping studies from SARS1 identified the minimum protein sequence necessary to bind to ACE2, a 196 amino acid region-the receptor binding domain (RBD), which is also found in SARS2. Binding studies with SARS1 and SARS2 RBDs showed roughly the same high affinity binding to ACE2, which does not correlate to viral transmission rates. One of the key differences in viral transmission rates is the addition of 12 nucleotides within the Spike protein creating a four amino acid RRAR-furin cleavage target after residue 684 allowing for pre-activation, splitting the protein into an Nt-S1 and Ct-S2 portions (38). The liberation of residues 1-684 (S1), containing the RBD from 333-529, likely provides easier access for binding to ACE2 and provide access for TMPRSS2 to cleave at the S2' border and reveal the S2 Fusion Peptide. It is thought that the RBD association with the ACE2 receptor provides proximity access to the plasma membrane located TMPRSS2; The S2 Fusion Peptide subsequently drives membrane fusion events for SARS1, SARS2 and NL63. The work here suggests that the RBD association with ACE2 may also take part in the virus transmission and/or internalization process.

Binding efficiencies and homologies between RBD across species.

There are 9 betacoronavirus and 1 alphacoronavirus with measured Kd of binding between RBD and ACE2. SARS1 and SARS2 have been measured at 58nM and 16nM respectively. High affinity is a trademark of most of these coronaviruses except for RaTG13 and RSYN06, which

bind in the micromolar range. The only alpha coronavirus that binds to ACE2, does so at 17nM, nearly identical to that of the SARS2 RBD. H-CoV-NL63 is a common human "cold virus" has not caused a worldwide pandemic, which again argues that affinity by itself does not correlate with virulence (39). Co-crystal studies with ACE2 comparing SARS1, SARS2 and NL63, despite a near complete lack of protein homology, reveal similarities in Nt and Internal region contacts on ACE2 (40). This parity of ACE2 contacts suggests that only certain regions on the protein can provide high affinity interactions and/or mediate ACE2 internalization, both of which may be critical to viral transmission.

An in vitro RBD-ACE2 binding assay.

It has recently been shown that SARS2 infection of the olfactory system is a critical step for infection to prosper (41). These results argue that propagation of the preliminary infection allow for both asymptomatic dissemination of the SARS2 virus as well as symptomatic consequences of deeper respiratory infections within ACE2/TMPRSS2 expressing cells that line the respiratory tract. If a compound can be identified to block the SARS2-Spike S1 binding to ACE2 in the olfactory epithelium, then it stands to reason viral transmission rates could be reduced. The in vitro system set up here robustly traffics RBD domains and ACE2 to the plasma membrane. The filopodia that exhibit RBD-β2AR-GFP fluorescence are 1μm or less, which is similar in size to the average size of a betacoronavirus particle 0.1 μm (42). Thus, some of the filopodial interactions with the plasma membrane (PM) of ACE2-Cherry expressing cells may indeed mimic viral particle binding. I used a range of RBDs with 1000-fold differences in published affinities, yet no difference was observed in the assay, consistent with pseudotype virus assays (43-45). Overall, our results mimic and extend the results obtained by pseudotype virus infection in cell lines and is likely higher throughput for sorting through the details of RBD binding to ACE2.

ACE2-Cherry protein relocalizes upon binding to RBD-β2AR

The RBD portion of spike proteins function by bringing its respective coronavirus to the PM where enzymes like TMPRSS2 cleave the spike protein liberating a S2 Fusion Peptide that functions to fuse viral and cellular membranes and enables endosome-independent entry (38). Here we observed a surprising finding that ACE2 by itself promotes internalization of RBD tethered to β2AR. In addition, rapid loss of ACE2-Cherry fluorescence could at the PM without formation of red/green doublet cells (**Figures 2D'**) suggests that reversable RBD binding is sufficient to trigger ACE2-Cherry loss. The mechanism of ACE2-Cherry loss is not known, but targeted degradation seems likely as other membrane localized proteins are not being lost (**Figures 3, S4**).

Meta-Analysis and mutational analysis of RBD reveal critical residues around disulfide Loop 4

The realization of a functional RBD-ACE2 interaction assay led to a meta-analysis of RBD mutations that were either derived from natural selection during infection (Variants) and DMS analysis by two laboratories (21, 28). Variants typically contain two or more mutations. By contrast DMS mutations are single substitutions of all 19 amino acids at each of the 197 residues of RBD, leading to an analysis of nearly 4000 mutants. DMS shows the distributed nature of

RBD binding to ACE2. The mapped RBM interface with ACE2 constitutes a 74 amino acid region. DMS meta-analysis suggests 7 residues are retained to establish binding to ACE2. Overall, 6 residues are predicted to have critical roles in the RBD double beta barrel configuration: Positively charged residues R454 and R509 likely connect to D667 and D442, respectively and neither are predicted to bind ACE2; residues C480 and C488 form the Loop 4 disulfide bond; and finally alpha helical breaking residues G502 and P507 that likely promote formation of the R509-D442 bridge. This leaves only N487 that would be absolutely necessary for binding and indeed is predicted to make contacts with both Nt proximal and distal residues Q24 and Y83, respectively. But the N487A mutation in RBD and both Q24A and Y83A mutations in ACE2 did not affect binding or internalization. Thus, none of these 7 residues would appear to confer the specificity of RBD-ACE2 binding.

Two additional analyses were performed looking at the most abundant mutations at multiple positions in the RBD in years 2020 (three) and four additional in 2021 (seven). Multiple alanine mutants at all seven positions K417, N439, L452, S477, T478, E484, and N501 affected binding or internalization by ACE2. A second set of multiple alanine substitutions were predicted (P.B.S.) in silico to be critical for binding: K417A, G446A, L455A, F486A, Q493A, Q498A, N501A. Indeed, binding and internalization are blocked. Two of these residues, L455 and F486 are not mutated in OM.BA.1, suggesting that one or both may be critical for binding. Reversion of residue 486 to phenylalanine in the P.B.S. 6 Ala mutant did indeed rescue RBD binding and internalization by ACE2. But the F486A mutation alone in RBD did not abolish binding and internalization. Thus, the totality of these alanine mutations, like the meta-analysis of the DMS, point to a distributed binding of RBD-ACE2.

The distributed nature of RBD binding seems antithetical to Kds with nanomolar affinities. DMS analyses of binding max studies reveal several residues G447, N448, Y449, N487, and Y489 that are critical for binding with Y489 being the most critical (30), yet Y449A, N487A did not affect binding and internalization; Y489A did prove critical. Juxtaposed to Y489 is the Loop 4 disulfide bond C480-C488 that is absent in the RBD RpYN06 that does not bind to ACE2. It seemed logical that this Loop 4 may be critically important for RBD binding or "attachment" to the Nt of ACE2. All Loop 4 residues between C480 to C488 were substituted with SARS1 and RaTG13 as well as alanine substitutions between F486 and L492. From all these swaps it did not appear that any one residue was key to the functionality of Loop 4, but rather supported the idea that formation of Loop 4 itself is critical. By contrast, blocking the formation of Loop 4 with the double alanine substitution of C480 and C488 prevented internalization of RBD by ACE2 expressing cells. Despite this result, it is not possible for Y489 alone to confer non-covalent high affinity binding to ACE2. Perhaps the disulfide Loop 4 is an anchor onto the Nt of ACE2 that was not observed by the crystallographic studies (1). Finally, DMS mutations (21, 28) would have predicted that N487A to be as debilitating as Y489A, which was not observe. Overall, the mutagenesis and meta-analysis failed to identify a contiguous stretch of a few residues that would bind ACE2.

The alphacoronavirus NL63 RBD that has a completely different primary sequencing and folding compared to RBDs of RaTG13, SARS1, and SARS2 as well as its RBM region is split over three surfaces, yet all bind similar regions on ACE2. But the amino acid identity is limited to just ten residues with of four of these surround the SARS2 Loop 4 region: C488 (C577 in NL63), F490,

P491 and L492; This region of NL63 RBD is not implicated in any RBM, but the N578Y mutation a generates a five amino acid match to SARS2 from C488-L492 and improves the NL63 RBD binding Kd 2-fold. In addition, the NL63 C577 residue is part of disulfide Loop 3 (**See Figure S6**). Taken together, the residues surrounding the disulfide Loop 4 in SARS2 is likely one of the critical regions for RBD interaction with ACE2. It is also possible that Loop 4 itself acts a hook onto the ACE2 amino terminus where it interacts (See Feinstein 2024b).

Odors as inhibitors to mitigate SARS-CoV-2 binding

The initial foray into studying RBD-ACE2 interactions was to identify an odor that could mitigate infections. None of the 36 odor mixtures from the "Le Nez du Café" were able to mitigate formation of RBD/ACE2 double positive cells nor ACE2 level of expression. A more directed approach could focus on the complete set of 4000 "relevant" odors for humans (https://ifrafragrance.org/priorities/ingredients/ifra-transparency-list) or the 230 Key Food Odors, and 800 common human odors (http://www.flavornet.org) that exist in everyday products.

A second approach searching for critical di or tri-peptide motifs within the 197 residue RBD also failed. But our mutagenesis identified the disulfide bridge between C480 and C488 as a tangible target. As we and other laboratories have shown, DTT and a more pH stable version DTBA could mitigate RBD/ACE2 binding. Both compounds are volatile and perceived as having a foul smell due to their thiol groups. These odors could be masked by sweet smelling odors. Additionally, there may be other odors that are more volatile and capable of disrupting the disulfide linkage, which could represent a viable solution to reduce rates of infections by a inhalation regimen.

Vaccines provide IgG responses that can limit viral amplifications, but unfortunately, mucosal protection (IgA) in the nasal epithelium wanes more quickly (46). Thus, most individuals are not immune to infection and the subsequent viral amplification within the sustentacular cells that carry ACE2 and TMPRSS2 expression. If inhibitors can block viral insult (7), then extent of disease would likely be mitigated as well.

Implications:

ACE2 down regulation: The rapid down regulation by a membrane bound RBD independent of stable binding, suggests that the efficiency of RBD binding and internalization might limit availability of ACE2 protein for future infections. Thus, the more downregulation that occurs for ACE2 prior to S2' liberation of the Fusion Peptide, might lead to fewer viral particles that can infect those target cells. We do not know the rate of *in vivo* ACE2 internalization by RBD and its eventual replacement to the plasma membrane, but this could be studied in the future using mice expressing the human ACE2 protein. Our binding assay reveals properties of RBD distinct from other observations that show the SARS2 pseudotype virus causing ACE2 degradation (47-49). It seems plausible that vaccines using RBD domains capable of binding ACE2 may lead to unwanted side effects produced from down regulation of ACE2 in recipients. In this regard, Pfizer produced several versions of RBD vaccines; if this hypothesis is true, then observed vaccine side effects may have similarities to some of the COVID-19 symptoms. It is notable that the full-length Spike protein has fewer side effects than just the RBD alone (50, 51). It is worth

exploring the possibility of fewer sides effects with vaccines expressing RBD containing mutations such as Y489A, the P.B.S. 7 Ala, C480A, C488A double mutant, or others (Feinstein 2024b) that reduce binding to ACE2.

Materials and Methods:

RBD and ACE2 constructs: See details of DNA sequences in **Supplemental Data File S1**. D1794 (is the beta2AR with an internal EcoR1 site added (does not alter residue) for rapid cloning of 5'ends. ACE2-Cherry (human ACE2 coding sequence with an internal EcoR1 site mutation (does not alter residues). RBD and ACE2 mutants made by gblocks (IDT) and sequenced after subcloning (see **Supplemental Data File S1**). SARS1 RBD from (19), SARS2 and RaTG13 are equivalent regions. NL63 RBD from NCBI. All RBD variants have been codon optimized.

hemagglutinin-cleavable signal sequence: (MKTIIALSYIFCLVFA) was initially used to test secreted version (21). All membrane tethered Nt RBD constructs used nicotinic receptor α7 subunit signal peptide: (MGLRALMLWLLAATGLVRESLQGEFQRKLYPVATM) (24, 25).

Cell culture and Imaging:
We have previously characterized β2AR and odorant receptor fluorescent protein fusions(16-18). Cells grown at 33°C and imaged 16hrs post-transfection. Typically, 15ug of DNA was electroporated (EPd) into 0.5 million OP6 cells. Imaging performed LSM510 confocal microscope or Spinning Disk microscope as previously performed (16).

RBD/ACE2 Interaction analysis:

- **In vitro co-plate binding assay**: RBD and ACE2 DNA constructs were separately EPd into OP6 cells, seeded (co-plated) onto the same 30cm^2 dishes, and imaged after 16hrs. Internalization of green fluorescence by red cells was obvious whether or not green cells were in close proximity. When internalization was not observed, then images were captured for at least 3 cells where Green/Red cells are touching**.**
- **In vitro co-EP assay:** 10ug of RBD and 10ug of ACE2 DNA constructs were Co-EPd into OP6 cells, seeded onto 30cm^2 dishes, and imaged after 1µ6hrs. At least 3 coexpressing cells were imaged for each.
- **Dissociation-Plate-FACs (*DPF*) assay:** 15ug of RBD and 15ug of ACE2 DNA constructs were separately EPd into OP6 cells and seeded onto different 30cm^2 dishes. RBD cells were trypsinized and seeded for the desired time onto the 16hrs grown ACE2 expressing cells in 30cm^2 dishes, then trypsinized, spun down, resuspended, filtered and counted by FACs.
- **In solution binding assay:** 15ug of RBD and 15ug of ACE2 DNA constructs were separately EPd into OP6 cells and seeded onto different 30cm^2 dishes. Both RBD cells and ACE2 cells were trypsinized, spun down, resuspended in 300µl of media. 50µl of each population were mixed into an Eppendorf tube and put in a 37°C water bath for 10min to 1hr. A 10µl aliquot was pipetted onto coverslip and imaged. Images were taken such that many cells were in the field of view. If doublets formed, then it was apparent throughout the field of view.

FACS was performed using a Becton Dickinson Aria II equipped with 5 lasers (BD bioscience). Gates were drawn as determined by negative controls to separate positive and negative populations for each florescent protein. Typically, 300,000 events (yielding about 250,000 DAPI positive cells) were recorded for each FACS analysis, and the data was analyzed

using BD FACSDiva 9.0.1. Calculations and graphs were made in GraphPad Prism. Mean and standard deviations were derived in Excel. See **Supplemental Data File S2** for details.

β2AR antagonist:
CellAura fluorescent $\beta_2$antagonist [(±)-propranolol]**,** HB7820 from Hello Bio https://www.hellobio.com/cellaura-fluorescent-beta2-antagonist-propranolol.html?q=7820 (52).

His Tag Alexa Fluor® 488-conjugated Antibody Catalog #: IC050G from R&D systems.
2019-nCoV RBD, His tag Cat#40592-V08H from SinoBiologicals

Odors:
Le Nez du Café Revelation Kit Odors-36 Scent concentrations from Expresso Parts.

Acknowledgements:

Special thanks to Masayo Omura for providing logistical and intellectual support that helped drive the success of these experiments. Many thanks to Masayo Omura, Ivan Rodriguez, Sergio Bernal-Garcia and Thomas Bozza for advice on the experimental design and interpretation of results; Mary Slavinsky and Masayo Omura for technical support in plasmid production; Livia Johnson and Diana Bratu for advice on utilizing the spinning disk microscope; and Sergio Bernal -Garcia for help with GraphPad Prism and Fiji. Thanks to Ivan Rodriguez, Vince Racaniello, Masayo Omura, and Sergio Bernal Garcia for providing feedback on the manuscript. Tomas Baumgartner Manager, Flow Cytometry Core Facility, Weill Cornell Medicine for support on flow cytometry of single cells. GISAID (http://cov-glue-viz.cvr.gla.ac.uk/mutations.php) for SARS-CoV2 database. Many thanks to Delia Tomoiaga, Claude Rose Levine and Mark Levine for supporting my efforts to design novel experiments that might help tackle the pandemic of our lifetime. This work was supported by Hunter College and NIH grants# NIH R01 NS091439-01 and NIH R01 DC020764-01.

References:

1. Wang Q, Zhang Y, Wu L, Niu S, Song C, Zhang Z, Lu G, Qiao C, Hu Y, Yuen KY, Wang Q, Zhou H, Yan J, Qi J. Structural and Functional Basis of SARS-CoV-2 Entry by Using Human ACE2. Cell. 2020;181(4):894-904 e9. Epub 2020/04/11. doi: 10.1016/j.cell.2020.03.045. PubMed PMID: 32275855; PMCID: PMC7144619.
2. Perlman KMaS. Coronaviruses, Including Severe Acute Respiratory Syndrome (SARS) and Middle East Respiratory Syndrome (MERS)
. Mandell, Douglas, and Bennett's Principles and Practice of Infectious Diseases 2015
. 2015(Chapter 157):1928–36.e2. Epub 2014 Oct 31. doi: 10.1016/B978-1-4557-4801-3.00157-0 ; PMCID: PMC7151770.
3. Borah P, Deb PK, Al-Shar'i NA, Dahabiyeh LA, Venugopala KN, Singh V, Shinu P, Hussain S, Deka S, Chandrasekaran B, Jaradat DMM. Perspectives on RNA Vaccine Candidates for COVID-19. Front Mol Biosci. 2021;8:635245. Epub 2021/04/20. doi: 10.3389/fmolb.2021.635245. PubMed PMID: 33869282; PMCID: PMC8044912.
4. Park JW, Lagniton PNP, Liu Y, Xu RH. mRNA vaccines for COVID-19: what, why and how. Int J Biol Sci. 2021;17(6):1446-60. Epub 2021/04/29. doi: 10.7150/ijbs.59233. PubMed PMID: 33907508; PMCID: PMC8071766.
5. Drozdzal S, Rosik J, Lechowicz K, Machaj F, Szostak B, Przybycinski J, Lorzadeh S, Kotfis K, Ghavami S, Los MJ. An update on drugs with therapeutic potential for SARS-CoV-2 (COVID-19) treatment. Drug Resist Updat. 2021;59:100794. Epub 2022/01/08. doi: 10.1016/j.drup.2021.100794. PubMed PMID: 34991982; PMCID: PMC8654464.
6. Killingley B, Mann AJ, Kalinova M, Boyers A, Goonawardane N, Zhou J, Lindsell K, Hare SS, Brown J, Frise R, Smith E, Hopkins C, Noulin N, Londt B, Wilkinson T, Harden S, McShane H, Baillet M, Gilbert A, Jacobs M, Charman C, Mande P, Nguyen-Van-Tam JS, Semple MG, Read RC, Ferguson NM, Openshaw PJ, Rapeport G, Barclay WS, Catchpole AP, Chiu C. Safety, tolerability and viral kinetics during SARS-CoV-2 human challenge in young adults. Nat Med. 2022;28(5):1031-41. Epub 2022/04/02. doi: 10.1038/s41591-022-01780-9. PubMed PMID: 35361992.
7. Shapira T, Monreal IA, Dion SP, Buchholz DW, Imbiakha B, Olmstead AD, Jager M, Desilets A, Gao G, Martins M, Vandal T, Thompson CAH, Chin A, Rees WD, Steiner T, Nabi IR, Marsault E, Sahler J, Diel DG, Van de Walle GR, August A, Whittaker GR, Boudreault PL, Leduc R, Aguilar HC, Jean F. A TMPRSS2 inhibitor acts as a pan-SARS-CoV-2 prophylactic and therapeutic. Nature. 2022;605(7909):340-8. Epub 2022/03/29. doi: 10.1038/s41586-022-04661-w. PubMed PMID: 35344983; PMCID: PMC9095466 US10988505B2) that cover matriptase and other type II transmembrane serine proteases inhibitors for treating and preventing viral infections, respiratory disorders, inflammatory disorders, pain disorders, tissue disorders, hyperproliferative disorders, and disorders associated with iron overload. The remaining authors declare that they have no competing interests.
8. Hoffmann M, Kleine-Weber H, Schroeder S, Kruger N, Herrler T, Erichsen S, Schiergens TS, Herrler G, Wu NH, Nitsche A, Muller MA, Drosten C, Pohlmann S. SARS-CoV-2 Cell Entry Depends on ACE2 and TMPRSS2 and Is Blocked by a Clinically Proven Protease Inhibitor. Cell. 2020;181(2):271-80 e8. Epub 2020/03/07. doi: 10.1016/j.cell.2020.02.052. PubMed PMID: 32142651; PMCID: PMC7102627.
9. Han DP, Penn-Nicholson A, Cho MW. Identification of critical determinants on ACE2 for SARS-CoV entry and development of a potent entry inhibitor. Virology. 2006;350(1):15-25.

Epub 2006/03/03. doi: 10.1016/j.virol.2006.01.029. PubMed PMID: 16510163; PMCID: PMC7111894.
10. Jonsdottir HR, Dijkman R. Coronaviruses and the human airway: a universal system for virus-host interaction studies. Virol J. 2016;13:24. Epub 2016/02/08. doi: 10.1186/s12985-016-0479-5. PubMed PMID: 26852031; PMCID: PMC4744394.
11. Leon Fodoulian JT, Daniel Rossier, Madlaina Boillat, Chenda Kan, Véronique Pauli, Kristof Egervari, Johannes A. Lobrinus, Basile N. Landis, Alan Carleton, Ivan Rodriguez. SARS-CoV-2 receptor and entry genes are expressed by sustentacular cells in the human olfactory neuroepithelium. bioRxiv 20200331013268; doi: https://doiorg/101101/20200331013268. 2020.
12. David H. Brann TT, Caleb Weinreb, Marcela Lipovsek, Koen Van den Berge, Boying Gong, Rebecca Chance, Iain C. Macaulay, Hsin-jung Chou, Russell Fletcher, Diya Das, Kelly Street, Hector Roux de Bezieux, Yoon-Gi Choi, Davide Risso, Sandrine Dudoit, Elizabeth Purdom, Jonathan S. Mill, Ralph Abi Hachem, Hiroaki Matsunami, Darren W. Logan, Bradley J. Goldstein, Matthew S. Grubb, John Ngai, Sandeep Robert Datta. Non-neuronal expression of SARS-CoV-2 entry genes in the olfactory system suggests mechanisms underlying COVID-19-associated anosmia. bioRxiv 20200325009084; doi: https://doiorg/101101/20200325009084. 2020.
13. Brann DH, Tsukahara T, Weinreb C, Lipovsek M, Van den Berge K, Gong B, Chance R, Macaulay IC, Chou HJ, Fletcher RB, Das D, Street K, de Bezieux HR, Choi YG, Risso D, Dudoit S, Purdom E, Mill J, Hachem RA, Matsunami H, Logan DW, Goldstein BJ, Grubb MS, Ngai J, Datta SR. Non-neuronal expression of SARS-CoV-2 entry genes in the olfactory system suggests mechanisms underlying COVID-19-associated anosmia. Sci Adv. 2020;6(31). Epub 2020/09/17. doi: 10.1126/sciadv.abc5801. PubMed PMID: 32937591.
14. Fodoulian L, Tuberosa J, Rossier D, Boillat M, Kan C, Pauli V, Egervari K, Lobrinus JA, Landis BN, Carleton A, Rodriguez I. SARS-CoV-2 Receptors and Entry Genes Are Expressed in the Human Olfactory Neuroepithelium and Brain. iScience. 2020;23(12):101839. Epub 2020/12/01. doi: 10.1016/j.isci.2020.101839. PubMed PMID: 33251489; PMCID: PMC7685946.
15. Zazhytska M, Kodra A, Hoagland DA, Frere J, Fullard JF, Shayya H, McArthur NG, Moeller R, Uhl S, Omer AD, Gottesman ME, Firestein S, Gong Q, Canoll PD, Goldman JE, Roussos P, tenOever BR, Jonathan BO, Lomvardas S. Non-cell-autonomous disruption of nuclear architecture as a potential cause of COVID-19-induced anosmia. Cell. 2022;185(6):1052-64 e12. Epub 2022/02/19. doi: 10.1016/j.cell.2022.01.024. PubMed PMID: 35180380; PMCID: PMC8808699.
16. Bubnell J, Pfister P, Sapar ML, Rogers ME, Feinstein P. beta2 adrenergic receptor fluorescent protein fusions traffic to the plasma membrane and retain functionality. PLoS One. 2013;8(9):e74941. Epub 2013/10/03. doi: 10.1371/journal.pone.0074941. PubMed PMID: 24086401; PMCID: PMC3781101.
17. Bubnell J, Jamet S, Tomoiaga D, D'Hulst C, Krampis K, Feinstein P. In Vitro Mutational and Bioinformatics Analysis of the M71 Odorant Receptor and Its Superfamily. PLoS One. 2015;10(10):e0141712. Epub 2015/10/30. doi: 10.1371/journal.pone.0141712. PubMed PMID: 26513476; PMCID: PMC4626375.
18. Jamet S, Bubnell J, Pfister P, Tomoiaga D, Rogers ME, Feinstein P. In Vitro Mutational Analysis of the beta2 Adrenergic Receptor, an In Vivo Surrogate Odorant Receptor. PLoS One.

2015;10(10):e0141696. Epub 2015/10/30. doi: 10.1371/journal.pone.0141696. PubMed PMID: 26513247; PMCID: PMC4626089.
19. Wong SK, Li W, Moore MJ, Choe H, Farzan M. A 193-amino acid fragment of the SARS coronavirus S protein efficiently binds angiotensin-converting enzyme 2. J Biol Chem. 2004;279(5):3197-201. Epub 2003/12/13. doi: 10.1074/jbc.C300520200. PubMed PMID: 14670965; PMCID: PMC7982343.
20. Towler P, Staker B, Prasad SG, Menon S, Tang J, Parsons T, Ryan D, Fisher M, Williams D, Dales NA, Patane MA, Pantoliano MW. ACE2 X-ray structures reveal a large hinge-bending motion important for inhibitor binding and catalysis. J Biol Chem. 2004;279(17):17996-8007. Epub 2004/02/03. doi: 10.1074/jbc.M311191200. PubMed PMID: 14754895; PMCID: PMC7980034.
21. Chan KK, Dorosky D, Sharma P, Abbasi SA, Dye JM, Kranz DM, Herbert AS, Procko E. Engineering human ACE2 to optimize binding to the spike protein of SARS coronavirus 2. Science. 2020;369(6508):1261-5. Epub 2020/08/06. doi: 10.1126/science.abc0870. PubMed PMID: 32753553.
22. Khazaal S, Harb J, Rima M, Annweiler C, Wu Y, Cao Z, Abi Khattar Z, Legros C, Kovacic H, Fajloun Z, Sabatier JM. The Pathophysiology of Long COVID throughout the Renin-Angiotensin System. Molecules. 2022;27(9). Epub 2022/05/15. doi: 10.3390/molecules27092903. PubMed PMID: 35566253; PMCID: PMC9101946.
23. Keck T, Leiacker R, Riechelmann H, Rettinger G. Temperature profile in the nasal cavity. Laryngoscope. 2000;110(4):651-4. Epub 2000/04/14. doi: 10.1097/00005537-200004000-00021. PubMed PMID: 10764013.
24. Jeanneteau F, Diaz J, Sokoloff P, Griffon N. Interactions of GIPC with dopamine D2, D3 but not D4 receptors define a novel mode of regulation of G protein-coupled receptors. Mol Biol Cell. 2004;15(2):696-705. Epub 2003/11/18. doi: 10.1091/mbc.e03-05-0293. PubMed PMID: 14617818; PMCID: PMC329290.
25. Weill C, Ilien B, Goeldner M, Galzi JL. Fluorescent muscarinic EGFP-hM1 chimeric receptors: design, ligand binding and functional properties. J Recept Signal Transduct Res. 1999;19(1-4):423-36. Epub 1999/03/11. doi: 10.3109/10799899909036662. PubMed PMID: 10071775.
26. McMahon C, Scadding GK. Le Nez du Vin--a quick test of olfaction. Clin Otolaryngol Allied Sci. 1996;21(3):278-80. Epub 1996/06/01. doi: 10.1111/j.1365-2273.1996.tb01741.x. PubMed PMID: 8818503.
27. Lan J, Ge J, Yu J, Shan S, Zhou H, Fan S, Zhang Q, Shi X, Wang Q, Zhang L, Wang X. Structure of the SARS-CoV-2 spike receptor-binding domain bound to the ACE2 receptor. Nature. 2020;581(7807):215-20. Epub 2020/04/01. doi: 10.1038/s41586-020-2180-5. PubMed PMID: 32225176.
28. Starr TN, Greaney AJ, Hilton SK, Ellis D, Crawford KHD, Dingens AS, Navarro MJ, Bowen JE, Tortorici MA, Walls AC, King NP, Veesler D, Bloom JD. Deep Mutational Scanning of SARS-CoV-2 Receptor Binding Domain Reveals Constraints on Folding and ACE2 Binding. Cell. 2020;182(5):1295-310 e20. Epub 2020/08/26. doi: 10.1016/j.cell.2020.08.012. PubMed PMID: 32841599; PMCID: PMC7418704.
29. Jawad B, Adhikari P, Podgornik R, Ching WY. Key Interacting Residues between RBD of SARS-CoV-2 and ACE2 Receptor: Combination of Molecular Dynamics Simulation and Density Functional Calculation. J Chem Inf Model. 2021;61(9):4425-41. Epub 2021/08/25. doi: 10.1021/acs.jcim.1c00560. PubMed PMID: 34428371; PMCID: PMC8409146.

30. Harvey WT, Carabelli AM, Jackson B, Gupta RK, Thomson EC, Harrison EM, Ludden C, Reeve R, Rambaut A, Consortium C-GU, Peacock SJ, Robertson DL. SARS-CoV-2 variants, spike mutations and immune escape. Nat Rev Microbiol. 2021;19(7):409-24. Epub 2021/06/03. doi: 10.1038/s41579-021-00573-0. PubMed PMID: 34075212; PMCID: PMC8167834.
31. Li W, Sui J, Huang IC, Kuhn JH, Radoshitzky SR, Marasco WA, Choe H, Farzan M. The S proteins of human coronavirus NL63 and severe acute respiratory syndrome coronavirus bind overlapping regions of ACE2. Virology. 2007;367(2):367-74. Epub 2007/07/17. doi: 10.1016/j.virol.2007.04.035. PubMed PMID: 17631932; PMCID: PMC2693060.
32. Zhou H, Ji J, Chen X, Bi Y, Li J, Wang Q, Hu T, Song H, Zhao R, Chen Y, Cui M, Zhang Y, Hughes AC, Holmes EC, Shi W. Identification of novel bat coronaviruses sheds light on the evolutionary origins of SARS-CoV-2 and related viruses. Cell. 2021;184(17):4380-91 e14. Epub 2021/06/21. doi: 10.1016/j.cell.2021.06.008. PubMed PMID: 34147139; PMCID: PMC8188299.
33. Wu K, Chen L, Peng G, Zhou W, Pennell CA, Mansky LM, Geraghty RJ, Li F. A virus-binding hot spot on human angiotensin-converting enzyme 2 is critical for binding of two different coronaviruses. J Virol. 2011;85(11):5331-7. Epub 2011/03/18. doi: 10.1128/JVI.02274-10. PubMed PMID: 21411533; PMCID: PMC3094985.
34. Liu K, Pan X, Li L, Yu F, Zheng A, Du P, Han P, Meng Y, Zhang Y, Wu L, Chen Q, Song C, Jia Y, Niu S, Lu D, Qiao C, Chen Z, Ma D, Ma X, Tan S, Zhao X, Qi J, Gao GF, Wang Q. Binding and molecular basis of the bat coronavirus RaTG13 virus to ACE2 in humans and other species. Cell. 2021;184(13):3438-51 e10. Epub 2021/06/18. doi: 10.1016/j.cell.2021.05.031. PubMed PMID: 34139177; PMCID: PMC8142884.
35. Mancek-Keber M, Hafner-Bratkovic I, Lainscek D, Bencina M, Govednik T, Orehek S, Plaper T, Jazbec V, Bergant V, Grass V, Pichlmair A, Jerala R. Disruption of disulfides within RBD of SARS-CoV-2 spike protein prevents fusion and represents a target for viral entry inhibition by registered drugs. FASEB J. 2021;35(6):e21651. Epub 2021/05/19. doi: 10.1096/fj.202100560R. PubMed PMID: 34004056; PMCID: PMC8206760.
36. Grishin AM, Dolgova NV, Landreth S, Fisette O, Pickering IJ, George GN, Falzarano D, Cygler M. Disulfide Bonds Play a Critical Role in the Structure and Function of the Receptor-binding Domain of the SARS-CoV-2 Spike Antigen. J Mol Biol. 2022;434(2):167357. Epub 2021/11/16. doi: 10.1016/j.jmb.2021.167357. PubMed PMID: 34780781; PMCID: PMC8588607.
37. Lukesh JC, 3rd, Palte MJ, Raines RT. A potent, versatile disulfide-reducing agent from aspartic acid. J Am Chem Soc. 2012;134(9):4057-9. Epub 2012/02/23. doi: 10.1021/ja211931f. PubMed PMID: 22353145; PMCID: PMC3353773.
38. Peacock TP, Goldhill DH, Zhou J, Baillon L, Frise R, Swann OC, Kugathasan R, Penn R, Brown JC, Sanchez-David RY, Braga L, Williamson MK, Hassard JA, Staller E, Hanley B, Osborn M, Giacca M, Davidson AD, Matthews DA, Barclay WS. The furin cleavage site in the SARS-CoV-2 spike protein is required for transmission in ferrets. Nat Microbiol. 2021;6(7):899-909. Epub 2021/04/29. doi: 10.1038/s41564-021-00908-w. PubMed PMID: 33907312.
39. Rawat P, Jemimah S, Ponnuswamy PK, Gromiha MM. Why are ACE2 binding coronavirus strains SARS-CoV/SARS-CoV-2 wild and NL63 mild? Proteins. 2021;89(4):389-98. Epub 2020/11/20. doi: 10.1002/prot.26024. PubMed PMID: 33210300; PMCID: PMC7753379.
40. Wu K, Li W, Peng G, Li F. Crystal structure of NL63 respiratory coronavirus receptor-binding domain complexed with its human receptor. Proc Natl Acad Sci U S A.

2009;106(47):19970-4. Epub 2009/11/11. doi: 10.1073/pnas.0908837106. PubMed PMID: 19901337; PMCID: PMC2785276.
41. Tang AT, Buchholz DW, Szigety KM, Imbiakha B, Gao S, Frankfurter M, Wang M, Yang J, Hewins P, Mericko-Ishizuka P, Leu NA, Sterling S, Monreal IA, Sahler J, August A, Zhu X, Jurado KA, Xu M, Morrisey EE, Millar SE, Aguilar HC, Kahn ML. Cell-autonomous requirement for ACE2 across organs in lethal mouse SARS-CoV-2 infection. PLoS Biol. 2023;21(2):e3001989. Epub 2023/02/07. doi: 10.1371/journal.pbio.3001989. PubMed PMID: 36745682; PMCID: PMC9934376.
42. Astuti I, Ysrafil. Severe Acute Respiratory Syndrome Coronavirus 2 (SARS-CoV-2): An overview of viral structure and host response. Diabetes Metab Syndr. 2020;14(4):407-12. Epub 2020/04/27. doi: 10.1016/j.dsx.2020.04.020. PubMed PMID: 32335367; PMCID: PMC7165108.
43. Li Y, Wang H, Tang X, Fang S, Ma D, Du C, Wang Y, Pan H, Yao W, Zhang R, Zou X, Zheng J, Xu L, Farzan M, Zhong G. SARS-CoV-2 and Three Related Coronaviruses Utilize Multiple ACE2 Orthologs and Are Potently Blocked by an Improved ACE2-Ig. J Virol. 2020;94(22). Epub 2020/08/28. doi: 10.1128/JVI.01283-20. PubMed PMID: 32847856; PMCID: PMC7592233.
44. Conceicao C, Thakur N, Human S, Kelly JT, Logan L, Bialy D, Bhat S, Stevenson-Leggett P, Zagrajek AK, Hollinghurst P, Varga M, Tsirigoti C, Tully M, Chiu C, Moffat K, Silesian AP, Hammond JA, Maier HJ, Bickerton E, Shelton H, Dietrich I, Graham SC, Bailey D. The SARS-CoV-2 Spike protein has a broad tropism for mammalian ACE2 proteins. PLoS Biol. 2020;18(12):e3001016. Epub 2020/12/22. doi: 10.1371/journal.pbio.3001016. PubMed PMID: 33347434; PMCID: PMC7751883.
45. Mou H, Quinlan BD, Peng H, Liu G, Guo Y, Peng S, Zhang L, Davis-Gardner ME, Gardner MR, Crynen G, DeVaux LB, Voo ZX, Bailey CC, Alpert MD, Rader C, Gack MU, Choe H, Farzan M. Mutations derived from horseshoe bat ACE2 orthologs enhance ACE2-Fc neutralization of SARS-CoV-2. PLoS Pathog. 2021;17(4):e1009501. Epub 2021/04/10. doi: 10.1371/journal.ppat.1009501. PubMed PMID: 33836016; PMCID: PMC8059821 following competing interests: M.F., H.M. and B.D.Q had filed a patent for the application of ACE2-Fc variants as a SARS-CoV-2 treatment. M.R.G., C.C.B., M.D.A., and M.F. are all cofounders of, and have an equity interest in Emmune Inc., a biotech company that specializes in the development of antibody-like antiviral therapies.
46. Havervall S, Marking U, Svensson J, Greilert-Norin N, Bacchus P, Nilsson P, Hober S, Gordon M, Blom K, Klingstrom J, Aberg M, Smed-Sorensen A, Thalin C. Anti-Spike Mucosal IgA Protection against SARS-CoV-2 Omicron Infection. N Engl J Med. 2022;387(14):1333-6. Epub 2022/09/15. doi: 10.1056/NEJMc2209651. PubMed PMID: 36103621; PMCID: PMC9511632.
47. Zamorano Cuervo N, Grandvaux N. ACE2: Evidence of role as entry receptor for SARS-CoV-2 and implications in comorbidities. Elife. 2020;9. Epub 2020/11/10. doi: 10.7554/eLife.61390. PubMed PMID: 33164751; PMCID: PMC7652413.
48. Sui Y, Li J, Venzon DJ, Berzofsky JA. SARS-CoV-2 Spike Protein Suppresses ACE2 and Type I Interferon Expression in Primary Cells From Macaque Lung Bronchoalveolar Lavage. Front Immunol. 2021;12:658428. Epub 2021/06/22. doi: 10.3389/fimmu.2021.658428. PubMed PMID: 34149696; PMCID: PMC8213020.
49. Ugo Bastolla1* PC, David Abia1, Maria-Laura Garcia-Bermejo3 and Manuel Fresno1. Is Covid-19 Severity Associated With ACE2 Degradation? Frontiers in Drug Discovery. 2022(January 2022 | Volume 1 | Article 789710). Epub 10.3389/fddsv.2021.789710.

50. Walsh EE, Frenck RW, Jr., Falsey AR, Kitchin N, Absalon J, Gurtman A, Lockhart S, Neuzil K, Mulligan MJ, Bailey R, Swanson KA, Li P, Koury K, Kalina W, Cooper D, Fontes-Garfias C, Shi PY, Tureci O, Tompkins KR, Lyke KE, Raabe V, Dormitzer PR, Jansen KU, Sahin U, Gruber WC. Safety and Immunogenicity of Two RNA-Based Covid-19 Vaccine Candidates. N Engl J Med. 2020;383(25):2439-50. Epub 2020/10/15. doi: 10.1056/NEJMoa2027906. PubMed PMID: 33053279; PMCID: PMC7583697.
51. Haas JW, Bender FL, Ballou S, Kelley JM, Wilhelm M, Miller FG, Rief W, Kaptchuk TJ. Frequency of Adverse Events in the Placebo Arms of COVID-19 Vaccine Trials: A Systematic Review and Meta-analysis. JAMA Netw Open. 2022;5(1):e2143955. Epub 2022/01/19. doi: 10.1001/jamanetworkopen.2021.43955. PubMed PMID: 35040967; PMCID: PMC8767431 scholarship from the German Academic Exchange Service (Deutscher Akademischer Austauschdienst) during the conduct of the study. No other disclosures were reported.
52. Ma G, Syu GD, Shan X, Henson B, Wang S, Desai PJ, Zhu H, Tao N. Measuring Ligand Binding Kinetics to Membrane Proteins Using Virion Nano-oscillators. J Am Chem Soc. 2018;140(36):11495-501. Epub 2018/08/17. doi: 10.1021/jacs.8b07461. PubMed PMID: 30114365; PMCID: PMC6211285.
53. Hati S, Bhattacharyya S. Impact of Thiol-Disulfide Balance on the Binding of Covid-19 Spike Protein with Angiotensin-Converting Enzyme 2 Receptor. ACS Omega. 2020;5(26):16292-8. Epub 2020/07/14. doi: 10.1021/acsomega.0c02125. PubMed PMID: 32656452; PMCID: PMC7346263.
54. Argentinian AntiCovid C. Structural and functional comparison of SARS-CoV-2-spike receptor binding domain produced in Pichia pastoris and mammalian cells. Sci Rep. 2020;10(1):21779. Epub 2020/12/15. doi: 10.1038/s41598-020-78711-6. PubMed PMID: 33311634; PMCID: PMC7732851.
55. Lin HX, Feng Y, Tu X, Zhao X, Hsieh CH, Griffin L, Junop M, Zhang C. Characterization of the spike protein of human coronavirus NL63 in receptor binding and pseudotype virus entry. Virus Res. 2011;160(1-2):283-93. Epub 2011/07/30. doi: 10.1016/j.virusres.2011.06.029. PubMed PMID: 21798295; PMCID: PMC7114368.
56. Temmam S, Vongphayloth K, Baquero E, Munier S, Bonomi M, Regnault B, Douangboubpha B, Karami Y, Chretien D, Sanamxay D, Xayaphet V, Paphaphanh P, Lacoste V, Somlor S, Lakeomany K, Phommavanh N, Perot P, Dehan O, Amara F, Donati F, Bigot T, Nilges M, Rey FA, van der Werf S, Brey PT, Eloit M. Bat coronaviruses related to SARS-CoV-2 and infectious for human cells. Nature. 2022;604(7905):330-6. Epub 2022/02/17. doi: 10.1038/s41586-022-04532-4. PubMed PMID: 35172323.

Figures:

Figure 1: An in vitro substitute for SARS2 virus binding to ACE2 expressing cells.
A. Experimental system to identify a compound that mitigates SARS2-RBD and ACE2 binding in cell lines. Expression vectors utilize EcoR1-PacI fusions of either SARS2-RBD variants or ACE2 to either mCherry or GFP fluorescent proteins. **B.-F.** Confocal images of separate electroporations into OP6 cells and co-plated overnight (O/N). All RBD constructs contain the nicotinic receptor α7 subunit (n) signal sequence at their N-termini **B.** Expression and co-plating of the first 60amino acids of β2AR (nTM1) to GFP and human ACE2 fused to mCherry. No double fluorescent cells observed: red (Cherry) and green (GFP). **C.** SARS2-RBD-β2AR-TM1 (nRBD-TM1) is fused to GFP and co-plated with ACE2-Cherry expressing cells. Red filopodia (16) are seen with green fluorescent on its distal points (see inset, magnification). **D.** Control co-plating of nβ2AR-GFP and ACE2-Cherry expressing cells show no double fluorescence. **E.** Control co-plating of the Delta variant, Delta-RBD-β2AR-GFP and β2AR-Cherry expressing show no double fluorescence. **F.** Co-plating Delta-RBD-β2AR-GFP and ACE2-Cherry expressing cells show dramatic internalization of GFP fluorescently tagged protein and no obvious morphology to the ACE2-Cherry expressing cells. Inset shows filopodia of ACE2-Cherry cells with GFP. Scale bars at 10μm**.**

Figure 2: Quantifying RBD-ACE2 interactions by single cell FACS analysis.
A and A'. Initial experiments aimed a quantifying interaction. RBD-TM1/ RBD-β2AR-GFP fusion constructs and controls co-plated after separate electroporation (EP) and left to interact for 16hrs. nTM1, SARS2-TM1, SARS2-TM1 plus overnight (O/N) LNDV odor mixture 35 (1:500), β2AR, SARS2, SARS2 plus LNDV odor mixture 35 (1:500), and two clones of Delta (1 and 2). In all cases where an RBD was present, double fluorescent cells were observed at 60x WT values, which were in the single digits. Data were performed in triplicate, but when all the WT or RBD containing cells are analyzed in aggregate, then highly statistically significant data is obtained. Surprisingly, ACE2 fluorescence was diminished in all cases RBD was present and again, when cells are analyzed in aggregate, data is highly significant. **B and B'.** Two double fluorescence cells shown by confocal imaging, revealing red cells with green speckles. **C-C''.** *Dissociated Cell-based Assay* Confocal imaging of a dissociated green cell adhering to a dissociated red cell that are acutely mixed for 10min at 37°C; Many of the cells were found to interact with an overt relocalization of the ACE2-Cherry protein (**C'**). **D and D'.** *Dissociate, Plate, FACs (DPF) Assay*. The speed of the interaction observed in **C**, was recapitulated by layering dissociating EPd test constructs on ACE2-cherry cells in triplicate including for 3 time points: 10min, 30min and 90min, followed by dissociation and FACs counting. ACE2-Cherry cells at all time points are from the same set of EPs were plated O/N on individual 30cm plates. GFP fluorescent cells, Control nβ2AR, SARS2-RBD and Delta-RBD cells were seeded onto sets of 30cm plates in triplicate. After O/N growth, individual 30cm plates of cells were trypsinized and plated on top of ACE2-Cherry cells for the defined time. Like the O/N co-cultures, the trypsinization-co-plating-FACs analysis revealed double fluorescence in 10min as well as a near 50% reduction in ACE2-Cherry fluorescence.

Figure 3: RBD-Cherry affects ACE2-GFP, but not gapFarred (see also Figure S4)

A-C. Confocal images for Co-EP of ACE2-GFP and gapFarred. After 16hrs Delta-RBD-Cherry cells are trypsinized and plated onto ACE2/gapFarred cells. **A-C'''**. In less than 10min after plating, aggregation of both Delta-RBD and ACE2 fusion proteins is observed, but not gapFarred. **D**. Histogram of fluorescence intensity changes in **C-C'''** also reveals aggregation of Delta-RBD and ACE2 fusion proteins, but not the membrane localized protein gapFarred. **E and E'.** *DPF Assay***,** FACs analysis of the Delta-RBD plated cells on ACE2-GFP cells for 90min reveals double fluorescent cells and a reduction of ACE2 expression relative to two controls, nβ2AR and CDH2**. F. F'.** Spinning disk confocal imaging of 10min acute coplating of O/N EPd ACE2-Cherry and Delta-RBD- nβ2AR-GFP cells reveal altered morphology of the red fluorescent cells, but not the green, fluorescent cells (**see also Movies S1A-C**).

Figure 4: RBD Meta-Analysis of Deep Mutational Screening, Identified Variants, Mutations Tested.
Alignment of SARS1 and SARS2 reveals 74% amino acid identity (145 residues) over the 197 residues of the Receptor Binding Domain (RBD). SARS2 Residue numbers from 333 to 529 are shown. Consensus residues are shown between SARS1 and SARS2**:** The + denoting similar amino acids (15 residues). Eight conserved Cysteine residues denoted by blue numbers and brackets with their proposed linkages: 1-1 (SARS2,336-361), 2-2 (SARS2,379-432), 3-3 (SARS2,391-525), 4-4 (SARS2,480-488) (53). Meta-analysis of Deep Mutational Screening of RBD reveals 29 residues (Red highlighted residues in the consensus) that are retained in 70% of the mutations and thus deemed immutable (21, 28). Orange highlighted residues or shaded regions in the consensus denote where mutations are found in SARS2 at a frequency greater than 0.03% or found in the omicron variant (http://cov-glue-viz.cvr.gla.ac.uk/mutations.php through 2021)(30); two residues are labelled with orange lettering as they reside among the highly conserved red highlighted residues, **Y449** and **G496**). In contrast to the variant residues, 9 red highlighted residues with green lettering, also denoted with green stars (G416, G431, R454, C480, N487, C488, G502, P507, R509) were deemed absolutely necessary, which include one pair of Cysteine residues C480-C488, three Glycines and one Proline that promote Beta turns and two Arginines that likely contribute to RBD structural integrity through interactions with conserved Aspartic Acid residues: black brackets (R355-D398 @2.8Å; D442-R509 @3.1Å; R454-D467 @3.4Å)(54) (54)**. Most of the red highlighted residues promote structural integrity of the RBD domain:** Red highlighted Glycines and Prolines are denoted with a red T, charged residues are denoted with red + or -, and hydrophobic residues are denoted with red H and polar Tyrosines/Serine with a red P.

Receptor Binding Motif (RBM): N437-R510 is underlined in SARS2. Amino acid differences are bolded with 5 Yellow highlighted residues (K417, F456, F486, Q493, Q498, N501) in SARS2 have been modeled by density function calculation to be the key residues that SARS2 tightly bind to ACE2 compared to SARS. Three residues Y449, N487 and Y489, highlighted in purple for SARS2 are predicted to be critical for strong association with ACE2.

RBD Variants Analyzed: RaTG13-RBD (blue residues predicted to be relevant for binding) (44), Delta variant-RBD **B.1.617.2**, Omicron variant-RBD **B.1.1.529 (OM.BA.1)**, Omicron variant-RBD **B.1.1.529.2 (OM.BA.2), BA.5,** and **Xbb1.5.**

Multiple Alanine Mutants analyzed to look at critical residues for RBM-ACE2 interaction: Predicted Binding Sites (P.B.S.): K417A, G446A, L455A, F486A, Q493A, Q498A, N501A, alters 4 of the modeled residues (bold), plus two additional residues implicated (27, 29). **P.B.S. 6 Ala:** returns F486 within Disulfide Loop 4 (480-488). **HiFrequency variations in 2020 SARS2 variants:** N439A, S477A, N501A **HiFrequency variations in 2021 SARS2 variants**: K417A, N439A, L452A, S477A, T478A, E484A, N501A

Figure 5: RBD Variants, Species Isoforms and Loop 4 mutants.
A, A'. RBD Variants and Species Isoforms: *DPF assay*. Three Variants of Concern were tested for their ability to bind and be internalized by ACE2: Delta, OM.BA.1 and OMBA.2 (not shown) and two species SARS1 and RaTG13 tested. All 5 of these RBDs were internalized by ACE2 in an indistinguishable manner, despite the measured binding of RaTG13 being 1000-fold less than SARS1 and SARS2. Four multiple alanine mutants were also tested (HiF2020, HiF2021, P.B.S. 7 Ala, P.B.S. 6 Ala). Neither the three-alanine mutation in HiF2020 nor the seven-alanine mutation in HiF2021 had any effect on RBD internalization by ACE2 cells. In contrast, the seven-alanine mutation in P.B.S. did abolish RBD binding. When F486A was reverted to WT, RBD internalization by ACE2 cells was readily observed. The divergent RBD in H-CoV-NL63 could function in the in vitro plate binding assay. NL63s(136 residues)-RBD is known to bind to similar domains on ACE2 through three non-contiguous RBM regions (**See Supplemental Figure S5, S6**). Indeed NL63-RBD was very efficient at being internalized by ACE2 cells. Single cell FACs binding assay scoring for reduction of ACE2 levels is inverse proportional to the formation of Red/Green cells. NL63-RBD was more robust at downregulating ACE2 than all other RBDs tested, which also accounts for the reduced number of Red/Green single cells. **B. Loop 4 mutants:** Meta-Analysis from DMS suggested that key Loop 4 Cysteines, N487 and Y489 were critical for RBM interaction with ACE2. Focusing in on Loop 4, both species Isoform substitutions as well as alanine scanning substitutions between F486 to L492. For comparative purposes, Y449A is tested. In O/N co-plating of constructs or by *DPF assay*, nearly all RBD species and alanine substitutions were internalized by ACE2 cells except for three: C488A and L492A, neither of which showed significant trafficking to the plasma membrane (PM); Y489A robustly trafficked to PM, bound, but was not internalized by ACE2 cells **(Supplemental Figure S8, S9)**. Single cell FACs binding assay parallels qualitative in vitro plate binding assay showing absence of Red/Green cells for P.B.S. mutant and near absence for Y489A. The P.B.S.+F486 nicely showed rescue. Based on cross species conservation, both Y489A and P491A were made in the OM.BA.1 variant, but unlike SARS2, both were unable to traffic to the PM **(Supplemental Figure S10)**.

Figure 6: Disulfide Bond Reducing Agents Block RBD-ACE2 Association.
A, B. *Dissociated Cell-based Assay*: SARS2-RBD (Green) or ACE2-Cherry (Red) by low magnification confocal microscopy which affords visualization of 10-15 Green and Red cells. Qualitative analysis of binding was performed after 90min incubation at 37°C for SARS2-RBD. Red/Green doublets (white arrows) were readily observed in at least 3 fields of view. Addition of 2mM DTT limits this interaction where doublets are rarely found. In contrast 2mM DTBA abolished the visualization of doublets (see inset). Both 2mM DTT and 2mM DTBA abolished doublet visualization for OM.BA.1-RBD as well. **C, C'**. *DPF assay*: NL63-RBD, which has a stronger effect on ACE2 expression was tested by 90min incubation. NL63-RBD shows both

increased numbers of Red/Green single cells, but also a decrease in ACE2 expression. By contrast addition of 2mM DTT abolished Red/Green single cells and ACE2 expression levels were not reduced.

Supplemental information inventory:

Supplemental Figures and legends:

S1 (relates to Figure 1): SARS2-RBD-B2AR-GFP incorporated membrane in ACE2 cells binds B2AR ligand.
S2 (relates to Figures 1 and 2): FACs Analysis of double positive cells and ACE2 levels in control experiments.
S3 (relates to Figures 1 and 2): Neither non-membrane bound RBD nor Xbb1.5 reduce ACE2-Cherry fluorescence.
S4 (relates to Figure 3): RBD-Venus affects ACE2-Cherry expression, but not gapTeal.
S5 (relates to Figure 4): Conservation of Disulfide Loop 4 Residues.
S6 (relates to Figures 4 and 5): NL63-RBD Alignment to SARS2-RBD.
S7 (relates to Figures 3 and S3): RpYN06 Alignment to SARS2-RBD.
S8 (relates to Figures 4 and 5): FACs Analysis of double positive cells and ACE2 levels for RBD mutants.
S9 (relates to Figure 5): Visualization of SARS2-RBD mutants in Cell-Based assay.
S10 (relates to Figures 4 and 5): Visualization of SARS2 and OM.BA.1-RBD mutants in Cell-Based assay.

Figure S1: SARS2-RBD-B2AR-GFP incorporated membrane in ACE2 cells binds B2AR ligand.
A. Schematic of protein interaction and a β2AR ligand binding**. B-B'''.** Overnight Delta-RBD-β2AR-GFP co-cultured with ACE2-Cherry cells. β2AR fluorescent ligand HB7820 (70nM, 1:500 dilution of 35μM stock) added to media for 10min and imaged. **B**. Green fluorescence from Delta-RBD-β2AR-GFP. **B'.** ACE2-Cherry expressing cells show Delta-RBD-β2AR-GFP internalized along with ACE2-Cherry. **B''.** β2AR ligand HB7820 fluorescence. **B'''.** Overlay shows β2AR ligand HB7820 bound to Delta-RBD-β2AR-GFP within ACE2 expressing cells (white arrowheads).

Figure S2: FACs Analysis of double positive cells and ACE2 levels in control experiments.
A-C and A'-C'. *DPF assay*: O/N transfection and FACs analysis of Co-plating GFP or Venus and Cherry expressing cells at either 90min (RBD cells trypsinized and added to ACE2 Cells or control cells. Green labeling represents GFP fusion proteins. Red labeling represents Cherry fusion proteins. Yellow labeling represents Venus fusion proteins. **A-C.** Data shows that double fluorescent cells are not found in the supernatant after co-plating, the cell adhesion protein CDH2 is efficient at generating double positive cells with no decreases to CHD2-Cherry nor ACE2-Cherry fluorescence. **A'-C'.** Data shows ACE2 fusion fluorescence for different test conditions. Critical finding from control experiments is the supernatant from Delta-RBD-β2AR-GFP expressing cells has no effect on ACE2 expressing cells.

Figure S3: Neither non-membrane bound RBD nor Xbb1.5 reduce ACE2-Cherry fluorescence.
A-A''. *DPF assay*. (This data makes up part of **Figure S6** in Feinstein 2024b) **A**. Double fluorescence after 90minute incubation of ACE2-Cherry cells with Ab488 (1μg/4mls of Goat-anti-HIS-Tag-Alexa488 Goat antibody [R&D#: IC050G]) with and without SinoRBD (60ng/4mls of 2019-nCoV-HisTag-RBD [Cat#40592-V08H; 234 residues, R319-F541]). **A'** ACE2-Cherry cells with Ab488 or Ab488+SinoRBD show no changes in fluorescence. **A''**. High expressing ACE2-Cherry fluorescence cells also show no changes in fluorescence. **Inset,** Shows ACE2-Cherry cell plus 240ng/5mls Sino-RBD. Punctate fluorescence is observed on the cell surface. **B.** Double fluorescence observed for NL63-RBD at 10min, 30min and 90min interaction with ACE2-Cherry plated cells. **B'.** ACE2-Cherry cells show reduced expression overall as well as cells highly expressing cells (red data points) when in contact with NL63 within 10min**.** Again nβ2AR controls show no difference. **C.** Double fluorescence is observed for SARS2-TM1, Xbb.15-RBD and NL63-RBD 90min interaction with ACE2-Cherry plated cells. **C'.** ACE2-Cherry cell fluorescence is reduced for SARS2-TM1 and NL63-RBD interactions, but not for Xbb.15-RBD. **C''.** ACE2-Cherry cells show reduced expression for highly expressing cells (red data points) in contact with SARS2-TM1 and NL63-RBD interactions, but not for Xbb.1.5-RBD.

Figure S4: RBD-Venus affects ACE2-Cherry expression, but not gapTeal.
A-A'''. Confocal images for Co-EP of ACE2-Cherrry and gapTeal co-plated with Delta-RBD-β2AR-Venus cells from acute trypsinization. **A-A'''**. In less than 30min, aggregation of both Delta-RBD and ACE2 fusion proteins is observed (white arrows). **B**. Histogram of fluorescence intensity changes also reveals aggregation of Delta-RBD and ACE2 fusion proteins, but not the membrane localized protein gapTeal. **C-C'''.** 16hr co-plating also shows gapTeal stays membrane bound despite all of ACE2-Cherry fusion protein found in aggregates. **D-D'''.** Co-EP of ACE2-Cherrry and gapTeal co-plated O/N with β2AR-Venus cells. No aggregation of β2AR-Venus and ACE2-Cherry protein.

Figure S5: Conservation of Disulfide Loop 4 Residues.
A curious finding by Zhou and colleagues found that *Rhinolophus pusillus* virus RpYN06 had strong homology the SARS2 virus but did not contain the disulfide bridge homology between Cysteine-480 to 488 (Loop 4) (**See Supplemental Figure S7**); The *R. pusillus* RpYN06-RBD did not bind to ACE2 (32). The Loop 4 region that lies within the SARS2-RBM is well conserved among eleven betacoronavirus species, eight of which are known to bind to ACE2 (8, 21, 31-34, 55). The only homology between the alpha coronavirus NL63-RBD and SARS2-RBD overlaps the Loop 4 region (**See Supplemental Figure S9**). An N578Y mutation is able increases the NL63-RBD binding affinity to ACE2 despite this domain residing outside of the three RBMs. Conserved Cysteines are highlighted in red, Prolines are highlighted in dark blue, Glycines are highlighted in yellow, Conserved Asparagines, Tyrosines, and Leucines are highlighted in green.

Figure S6: NL63-RBD Alignment to SARS2-RBD.
Both NL63-RBD and SARS2-RBD domains both bind and are internalized by ACE2 expressing cells. NL63-RBD contains three RBM domains (grey highlighted regions) and three predicted disulfide bridges (green numbers and arrows), compared to one RBM for SARS2-RBD (yellow highlighted region) and two critical disulfide bridges (blue numbers and arrows). Manual alignment between 136 residue NL63-RBD and 197 residue SARS-RBD. Consensus sequence reveals only 10 amino acid identities. Four of these residues reside in a 5 amino acid stretch that overlaps Loop 4 region within the RBM of SARS2 (31). Loop 4 alignment in Figure S2 identifies conserved Glycines in Prolines between Cysteine residues. These residues (dark blue highlights) are also found in NL63 and in close proximity to the conserved CxFPL. It is worth noting that the N578Y mutation in NL63 bringing the identity to 5/5 identities CNFPL, doubles the binding affinity to ACE2 (**see Supplemental Figure S2**).

Figure S7: RpYN06 Alignment to SARS2-RBD.
The RaTG13 betacoronavirus is one of the most highly homologous betacaronaviruses to SARS2 sharing 96% overall identity including the RBM region (residue differences in brown). By contrast, RpYN06 has 95% nucleotide identity over the 30kb colinear genome, but its RBM region has lost nucleotide homology to SARS2 with the best stretch having 22/57 residues conserved (residue differences in blue). It is notable that two of the eight cysteines are not conserved (highlighted in red), and both make up disulfide Loop 4. Loss of RBM homology correlates with loss of ACE2 binding (32, 56).

Figure S8: FACs Analysis of double positive cells and ACE2 levels for RBD mutants.
A-C and A'-C'. Overnight (O/N) transfection and FACs analysis of Co-plating GFP and Cherry expressing cells at either 90min (RBD cells trypsinized and added to ACE2 Cells. Green labeling represents GFP fusion proteins. Red labeling represents Cherry fusion proteins. **A-B and A'-B'**. Data shows that double florescent cells are found with RBDs of SARS1, SARS2, Delta, Omicron, RaTG13, NL63; Concomitant loss of ACE2 expression was observed. The N487A mutant still robustly bound and ACE2 expression was unperturbed in contrast to Y489A where nearly all binding is abolished, but still shows reduced expression of ACE2. The 7Ala mutation of the Predicted Binding Site (P.B.S. 7Ala: K417A, G446A, L455A, F486A, Q493A, Q498A, N501A) completely abolished binding and no loss of ACE2 expression was observed. By contrast P.B.S. 6Ala mutation (+F486) generated substantial double positives as well as loss of ACE2 expression.

Figure S9: Visualization of SARS2-RBD mutants in Cell-Based assay.
A-F. Confocal images for co-plated RBD variants and mutants with ACE2-Cherry after 16hrs. **A and A'.** P.B.S. 7 Ala-RBD expressing cells reveal fluorescent filopodia at the membrane (obvious filopodia), but the protein is not found bound to ACE2-Cherry cells. **B.** P.B.S.6 Ala do bind ACE2-Cherry cells. **C.** SARS2-RBD expressing cells robustly bind ACE2-Cherry cells. **D.** N487A-RBD, **E and E'.** Y489A-RBD and **F and F'.** C480-C488A-RBD with ACE2-Cherry Cells. N487A-RBD interactions with ACE2-Cherry are robust, in contrast to Y489A-RBD and C440-C488A-RBDs which rarely interact with ACE2-Cherry Cells.

Figure S10: Visualization of SARS2 and OM.BA.1-RBD mutants in Cell-Based assay.
A-F. Low magnification confocal images for co-plated RBD variants and mutants with ACE2-Cherry reveals the pervasiveness of RBD-ACE2 interactions/noninteractions, RBD membrane trafficking/non-trafficking. **A.** SARS2-RBD protein is readily internalized by ACE2-Cherry cells and reduces its membrane expression. **B.** P.B.S. 7 Ala-RBD expressing cells are well expressed at the membrane (obvious filopodia), but the protein is not found bound to ACE2-Cherry cells. **C.** P.B.S. 6 Ala Shows binding ACE2-Cherry cells. **D.** Y489A-RBD expressing cells do not show binding to ACE2-Cherry cells. **E.** Y489A-OM.BA.1-RBD and **F.** P491A-OM.BA.1-RBD Show no filipodia and no interactions with ACE2-Cherry Cells.

Movie S1, S2, S3.
Spinning Disk 10minute Time Course between Delta-RBD-GFP cells and ACE2-Cherry Cells. **S1**. Flattened Z-Stack Overlay of 20 images (one/30 seconds). **S2**. Flattened Z-Stack Delta RBD-GFP. **S3**. Flattened Z-Stack ACE2-Cherry.

Figure 1

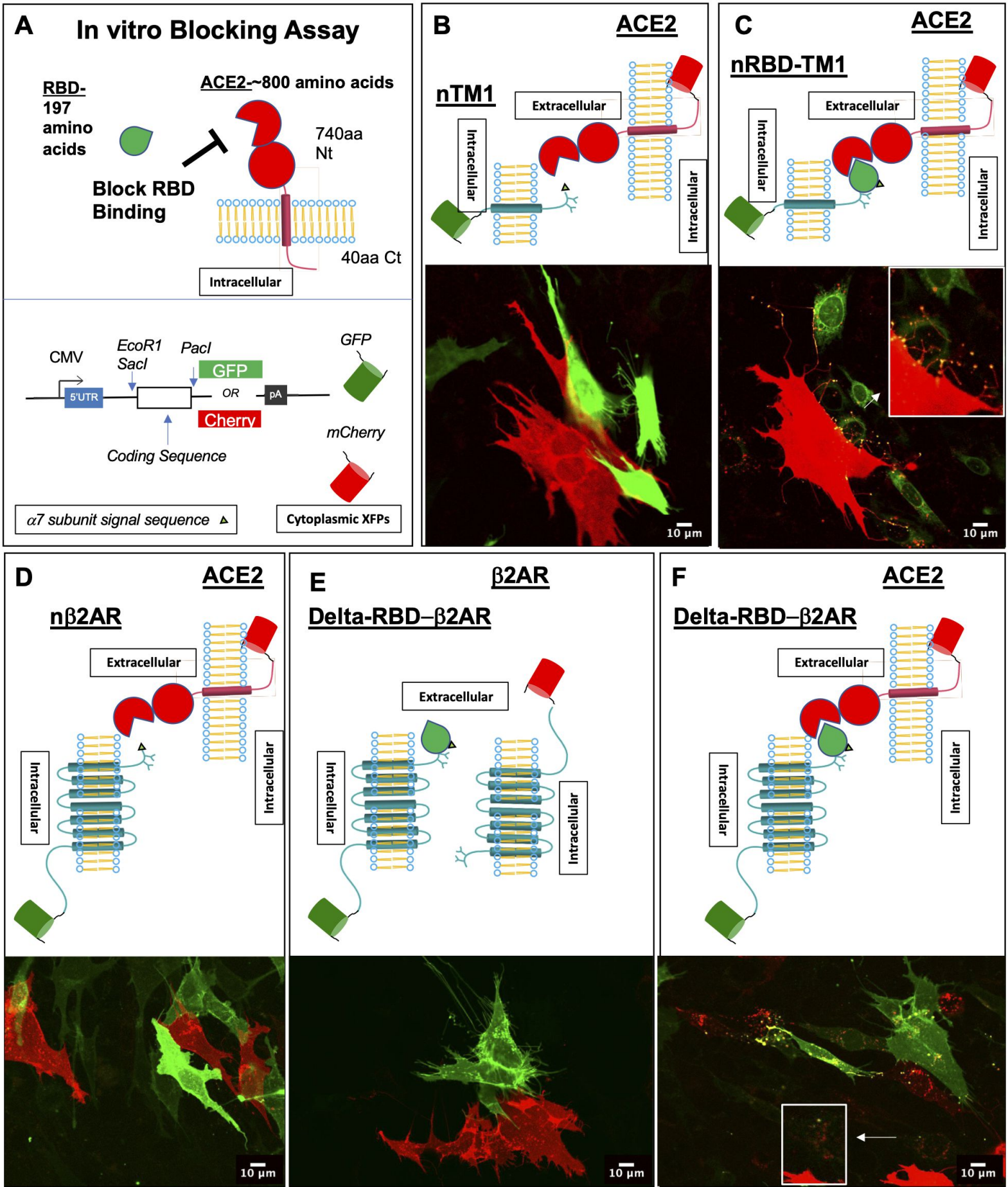
A
In vitro Blocking Assay
RBD-
197
amino
acids
ACE2-~800 amino acids
740aa
Nt
Block RBD
Binding
40aa Ct
Intracellular
CMV
EcoR1
SacI
PacI
GFP
5'UTR
OR
pA
Cherry
Coding Sequence
GFP
mCherry
α7 subunit signal sequence
Cytoplasmic XFPs
B
ACE2
nTM1
Extracellular
Intracellular
Intracellular
10 µm
C
ACE2
nRBD-TM1
Extracellular
Intracellular
Intracellular
10 µm
D
ACE2
nβ2AR
Extracellular
Intracellular
Intracellular
10 µm
E
β2AR
Delta-RBD–β2AR
Extracellular
Intracellular
Intracellular
10 µm
F
ACE2
Delta-RBD–β2AR
Extracellular
Intracellular
Intracellular
10 µm

Figure 2

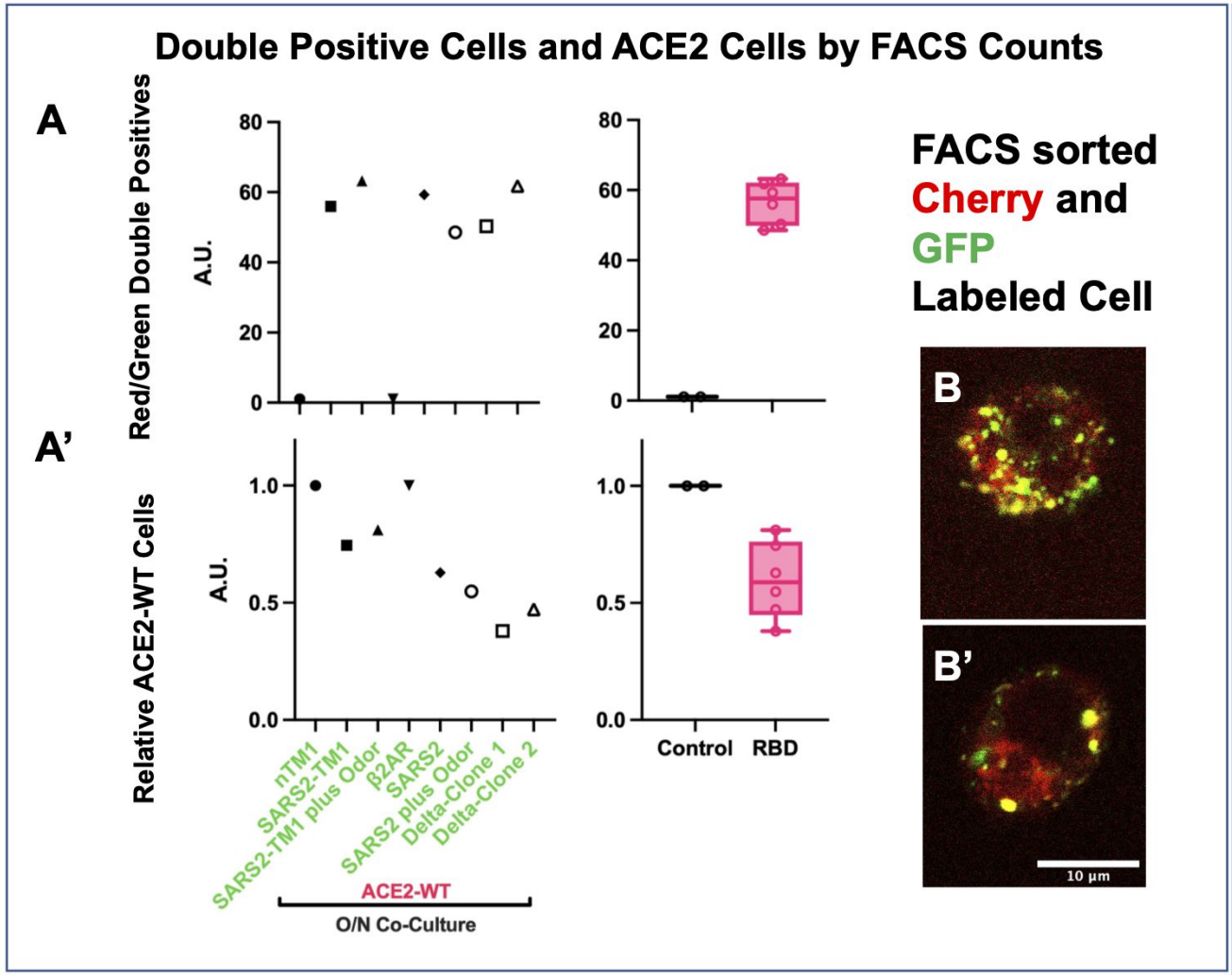
Double Positive Cells and ACE2 Cells by FACS Counts
A
A'
Red/Green Double Positives
Relative ACE2-WT Cells
A.U.
80
60
40
20
0
1.0
0.5
0.0
nTM1
SARS2-TM1
SARS2-TM1 plus Odor
β2AR
SARS2
SARS2 plus Odor
Delta-Clone 1
Delta-Clone 2
ACE2-WT
O/N Co-Culture
Control
RBD
FACS sorted
Cherry and
GFP
Labeled Cell
B
B'
10 µm

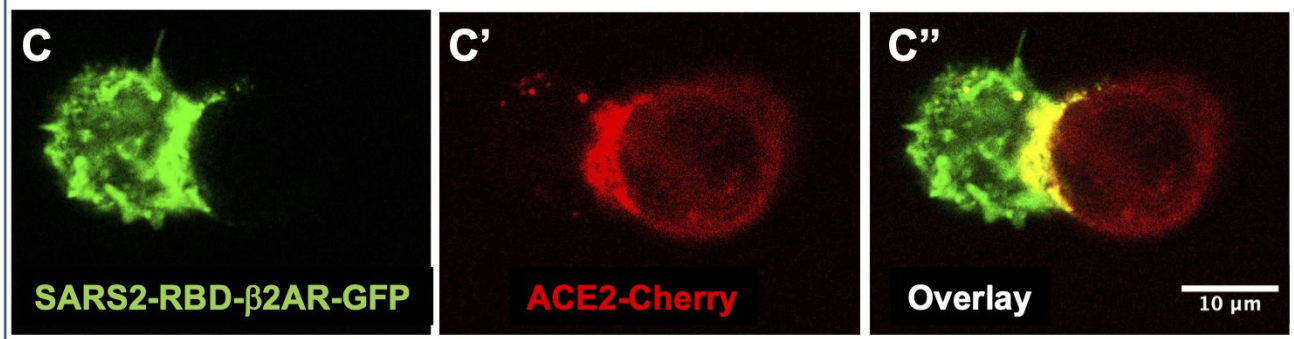
10min co-incubation in a tube shows rapid binding
C
C'
C''
SARS2-RBD-β2AR-GFP
ACE2-Cherry
Overlay
10 µm

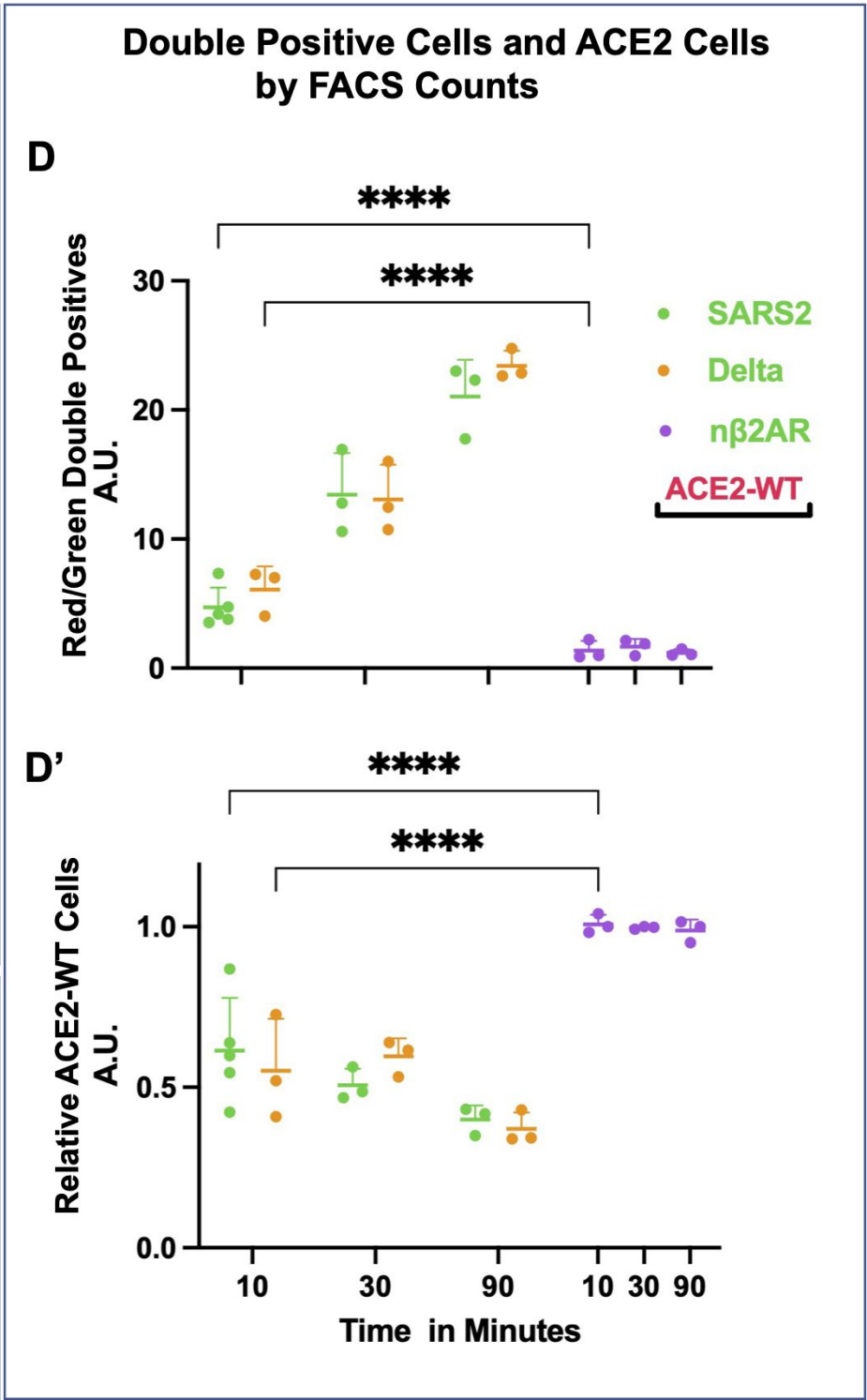
Double Positive Cells and ACE2 Cells
by FACS Counts
D
D'
****
****
Red/Green Double Positives
A.U.
30
20
10
0
SARS2
Delta
nβ2AR
ACE2-WT
Relative ACE2-WT Cells
A.U.
1.0
0.5
0.0
10
30
90
10
30
90
Time in Minutes

Figure 3

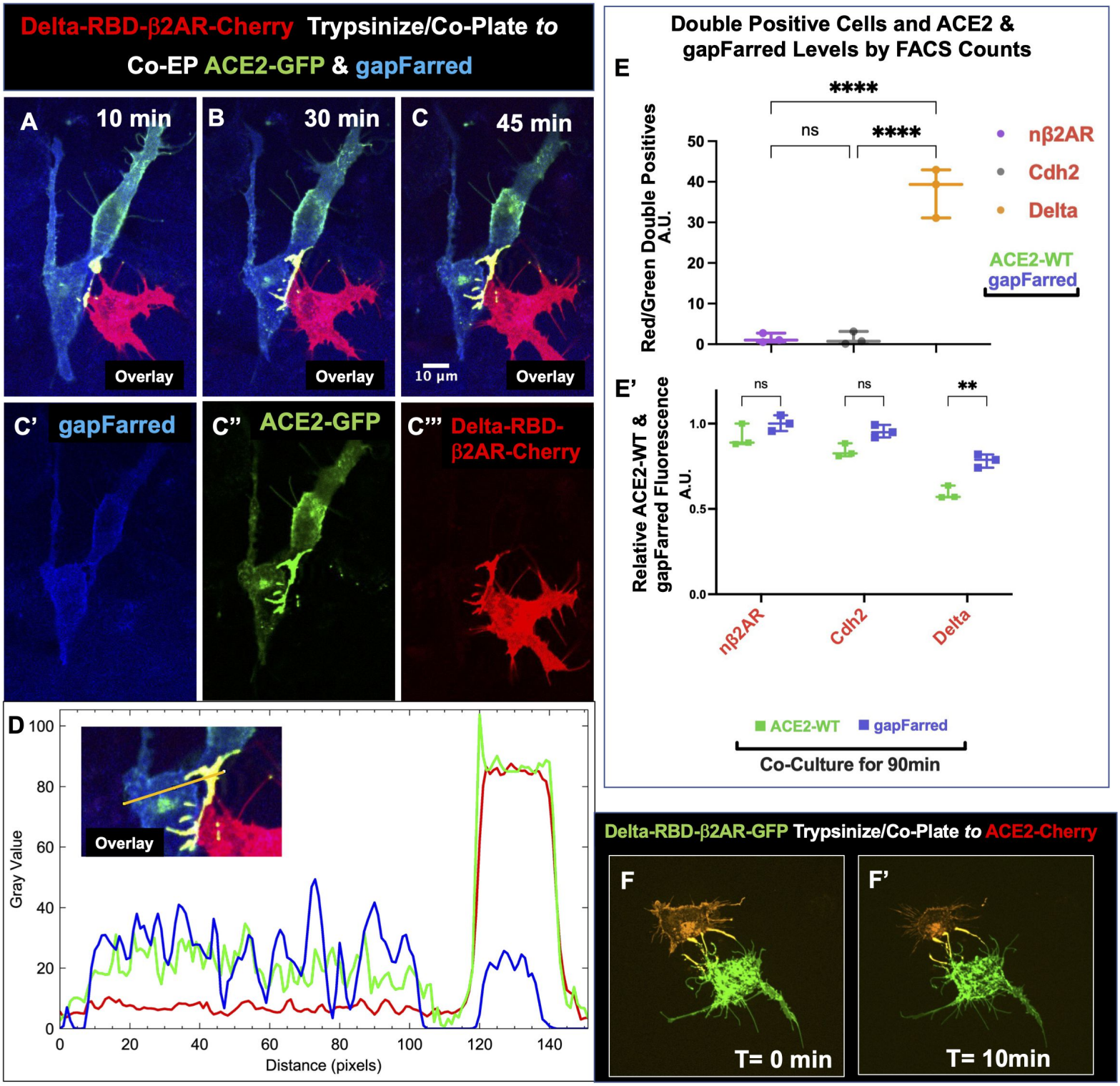
Delta-RBD-β2AR-Cherry Trypsinize/Co-Plate to Co-EP ACE2-GFP & gapFarred
A 10 min
B 30 min
C 45 min
Overlay
10 µm
C' gapFarred
C'' ACE2-GFP
C''' Delta-RBD-β2AR-Cherry
D
Gray Value
Distance (pixels)
Double Positive Cells and ACE2 & gapFarred Levels by FACS Counts
E
Red/Green Double Positives A.U.
****
ns
nβ2AR
Cdh2
Delta
ACE2-WT
gapFarred
E'
Relative ACE2-WT & gapFarred Fluorescence A.U.
ns
ns
**
ACE2-WT
gapFarred
Co-Culture for 90min
Delta-RBD-β2AR-GFP Trypsinize/Co-Plate to ACE2-Cherry
F
F'
T= 0 min
T= 10min

Figure 4

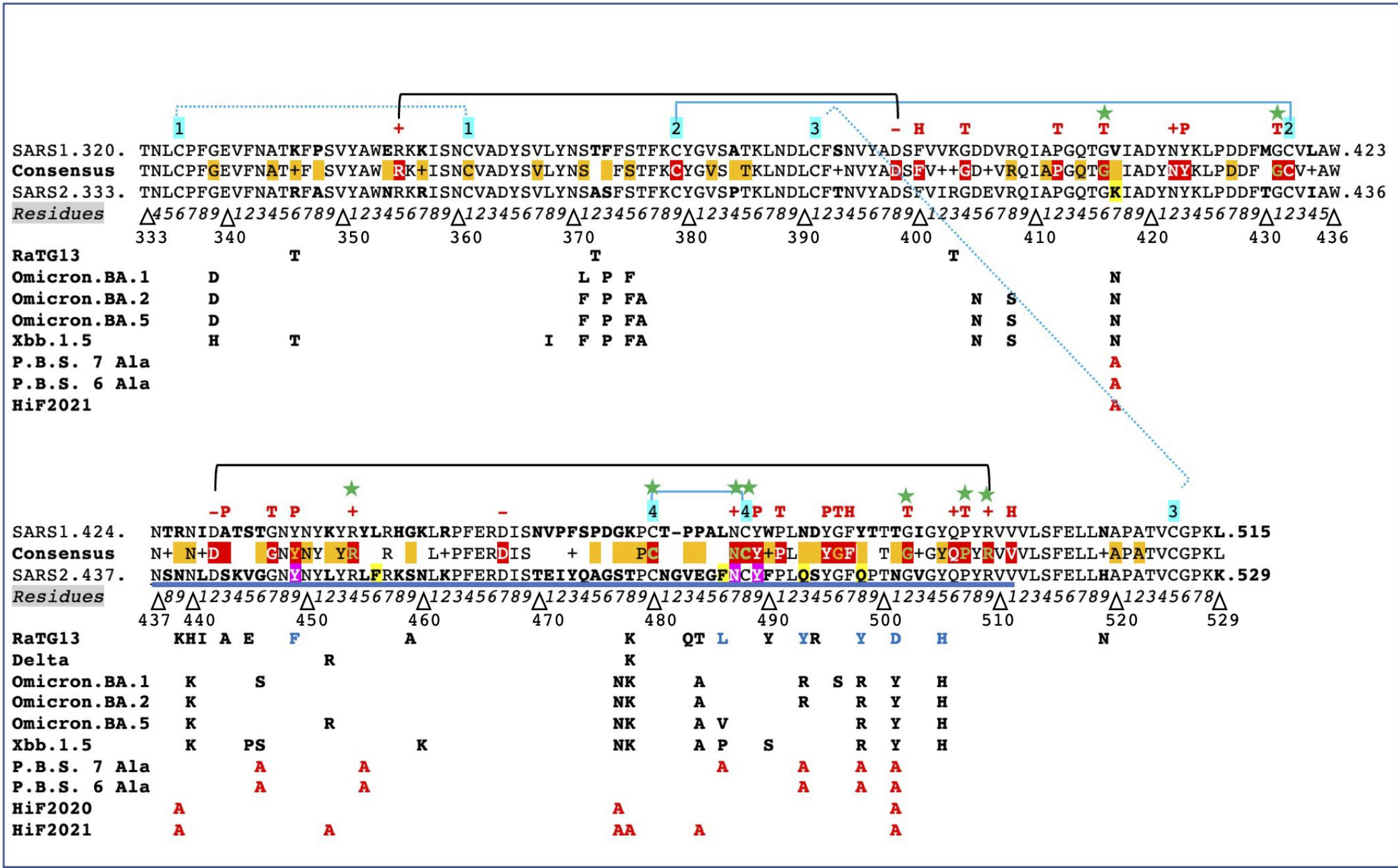
SARS1.320. TNLCPFGEVFNATKFPSVYAWERKKISNCVADYSVLYNSTFFSTFKCYGVSATKLNDLCFSNVYADSFVVKGDDVRQIAPGQTGVIADYNYKLPDDFMGCVLAW.423
Consensus TNLCPFGEVFNAT+F SVYAW RK+ISNCVADYSVLYNS FSTFKCYGVS TKLNDLCF+NVYADSFV++GD+VRQIAPGQTG IADYNYKLPDDF GCV+AW
SARS2.333. TNLCPFGEVFNATRFASVYAWNRKRISNCVADYSVLYNSASFSTFKCYGVSPTKLNDLCFTNVYADSFVIRGDEVRQIAPGQTGKIADYNYKLPDDFTGCVIAW.436
Residues
333 340 350 360 370 380 390 400 410 420 430 436
RaTG13
Omicron.BA.1
Omicron.BA.2
Omicron.BA.5
Xbb.1.5
P.B.S. 7 Ala
P.B.S. 6 Ala
HiF2021
SARS1.424. NTRNIDATSTGNYNYKYRYLRHGKLRPFERDISNVPFSPDGKPCT-PPALNCYWPLNDYGFYTTTGIGYQPYRVVVLSFELLNAPATVCGPKL.515
Consensus N+ N+D GNYNY YR R L+PFERDIS + PC NCY+PL YGF T G+GYQPYRVVVLSFELL+APATVCGPKL
SARS2.437. NSNNLDSKVGGNYNYLYRLFRKSNLKPFERDISTEIYQAGSTPCNGVEGFNCYFPLQSYGFQPTNGVGYQPYRVVVLSFELLHAPATVCGPKK.529
Residues
437 440 450 460 470 480 490 500 510 520 529
RaTG13
Delta
Omicron.BA.1
Omicron.BA.2
Omicron.BA.5
Xbb.1.5
P.B.S. 7 Ala
P.B.S. 6 Ala
HiF2020
HiF2021

Figure 5

Double Positive Cells and ACE2 Cells by FACS Counts

A

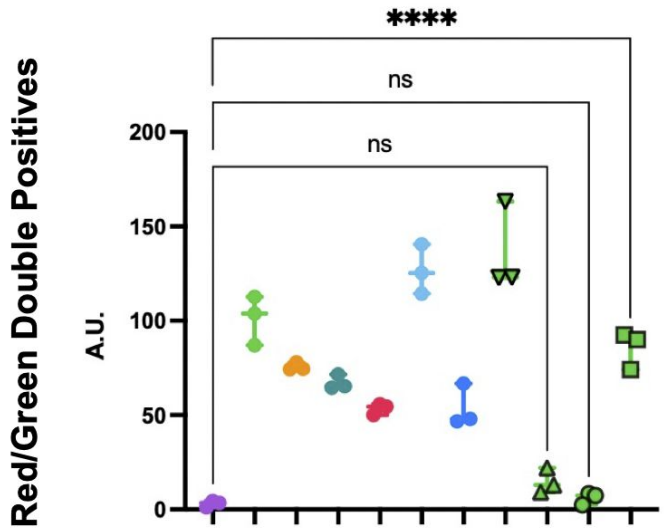

A'

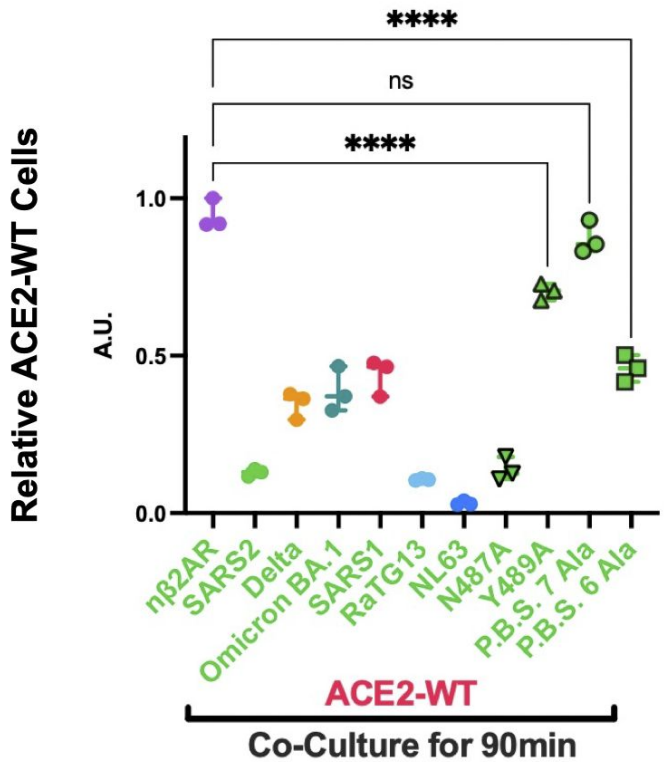

B

Loop 4 Region Mutations Tested

RBD Internalized

ACE2 WT	RBD
YES	SARS2
YES	T-PPAL(SARS1)
YES	QTL(RaTG13)
YES	F486A
YES	N487A
NO	C488A#
NO	C480A,C488A*
NO	Y489A*
YES	Y489W
YES	Y489H
YES	F490A
YES	P491A
NA	L492A^
YES	Y449A

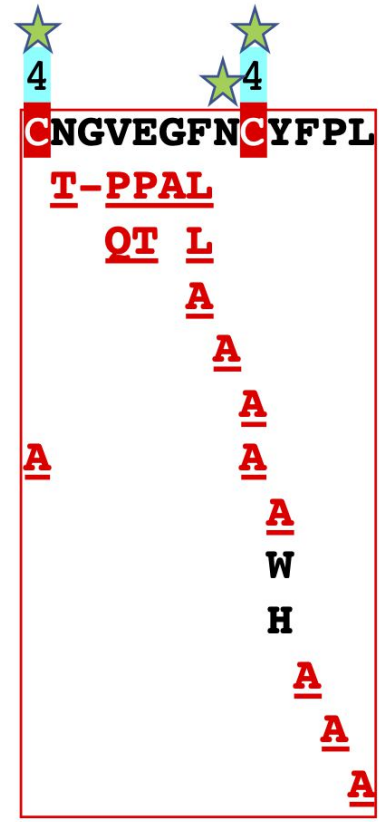

* Traffics well to plasma membrane

\# Poorly traffics to plasma membrane

^ NO trafficking to plasma membrane

Y489A or P491A point mutations in OM.BA.1. do not traffic to plasma membrane.

Figure 6

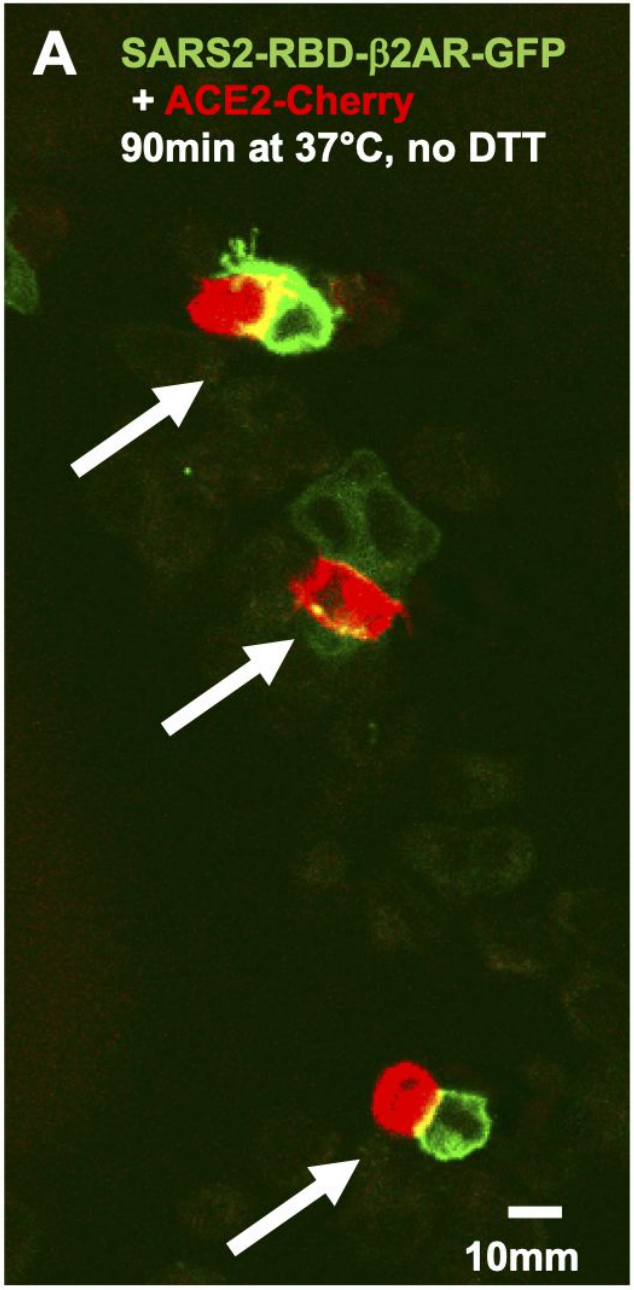

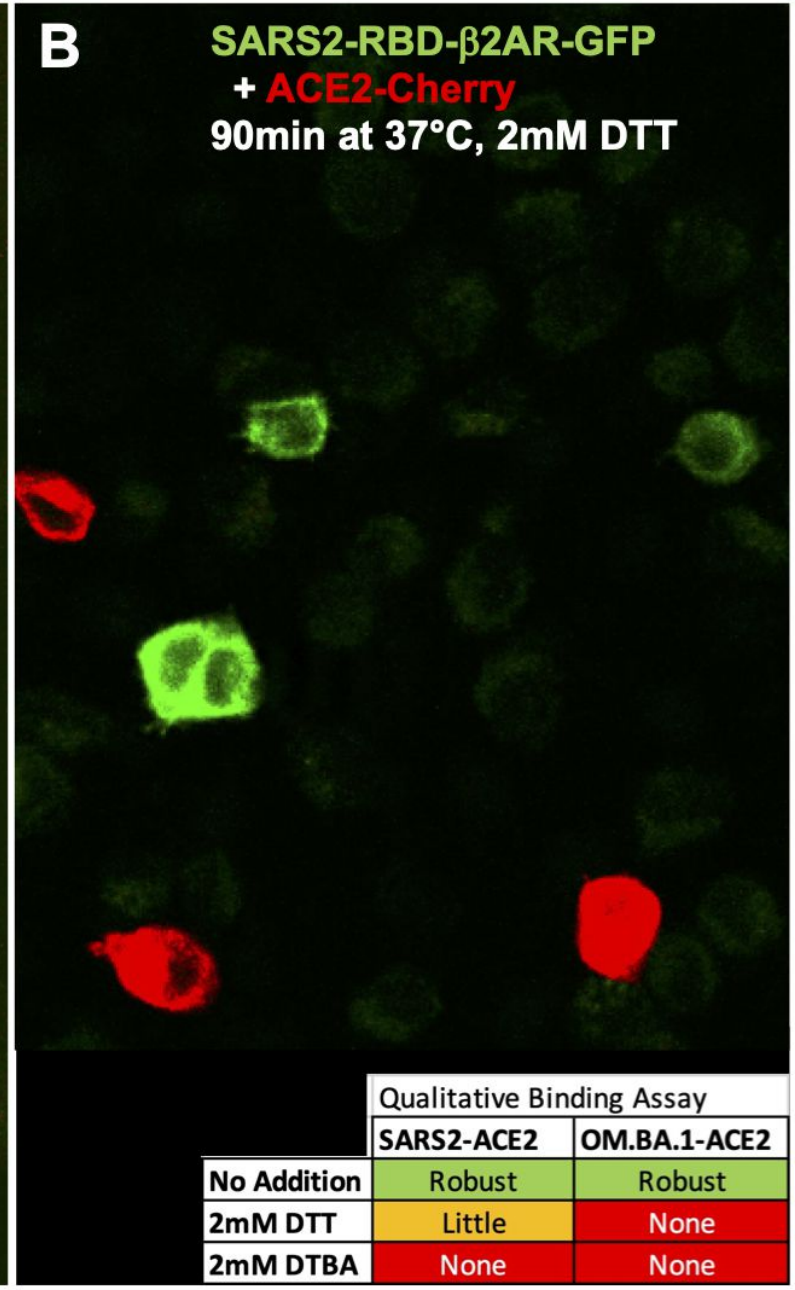

Qualitative Binding Assay

	SARS2-ACE2	OM.BA.1-ACE2
No Addition	Robust	Robust
2mM DTT	Little	None
2mM DTBA	None	None

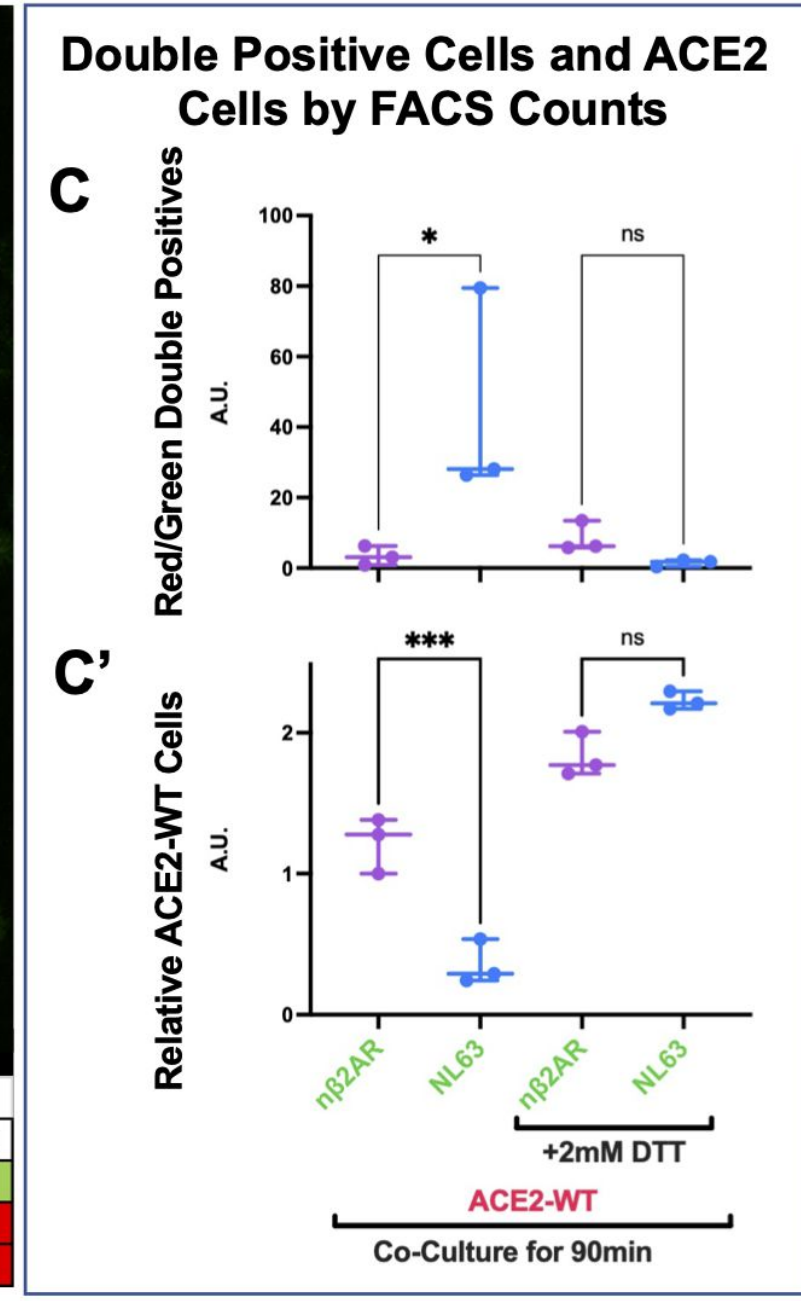

Figure S1

Internalized Membrane RBD–β2AR-GFP in ACE2-Cherry Cell Binds β2AR Ligand

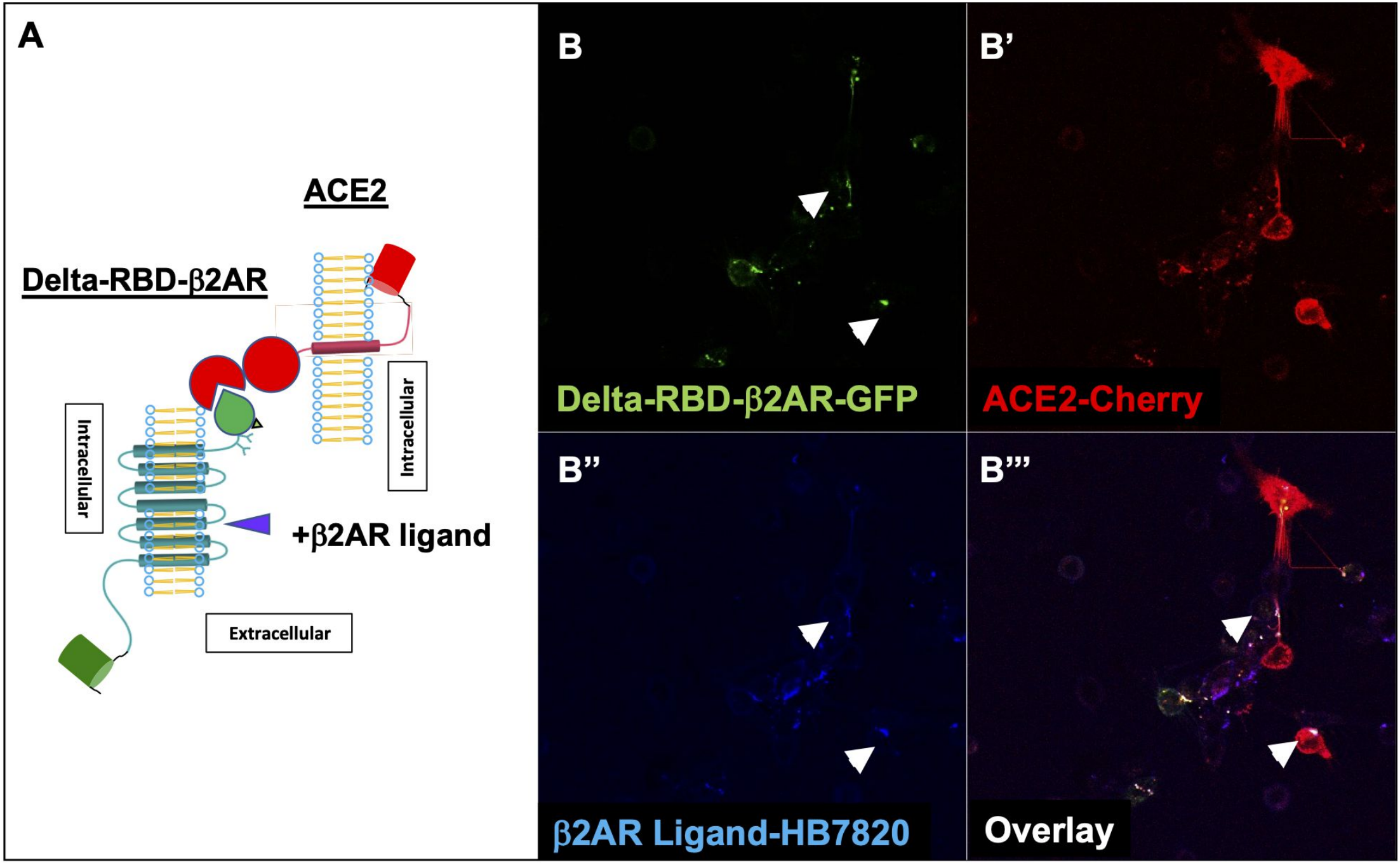

Figure S2

Controls for RBD and ACE2 *DPF assay*

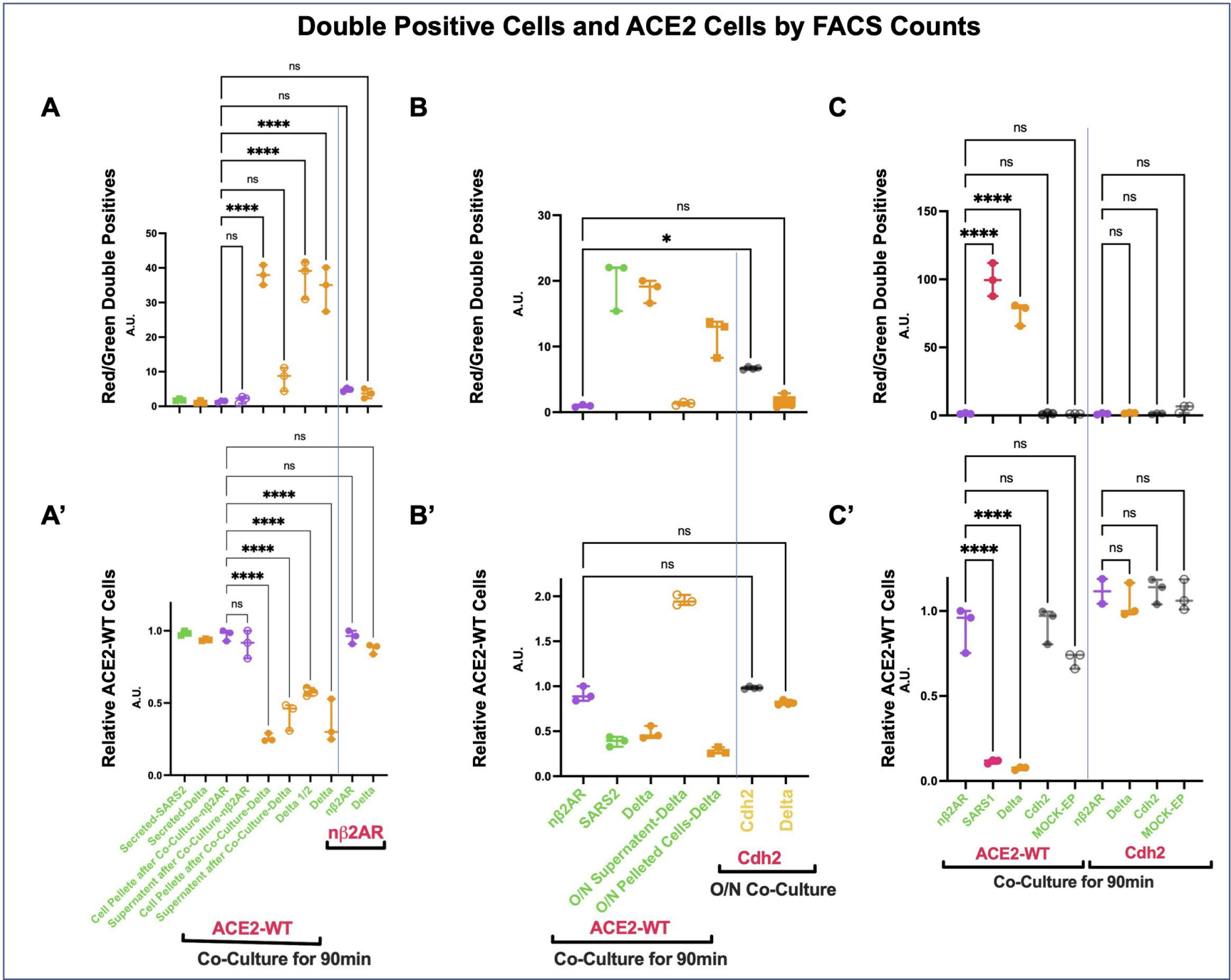

Figure S3

Additional controls for RBD and ACE2 *DPF assay*

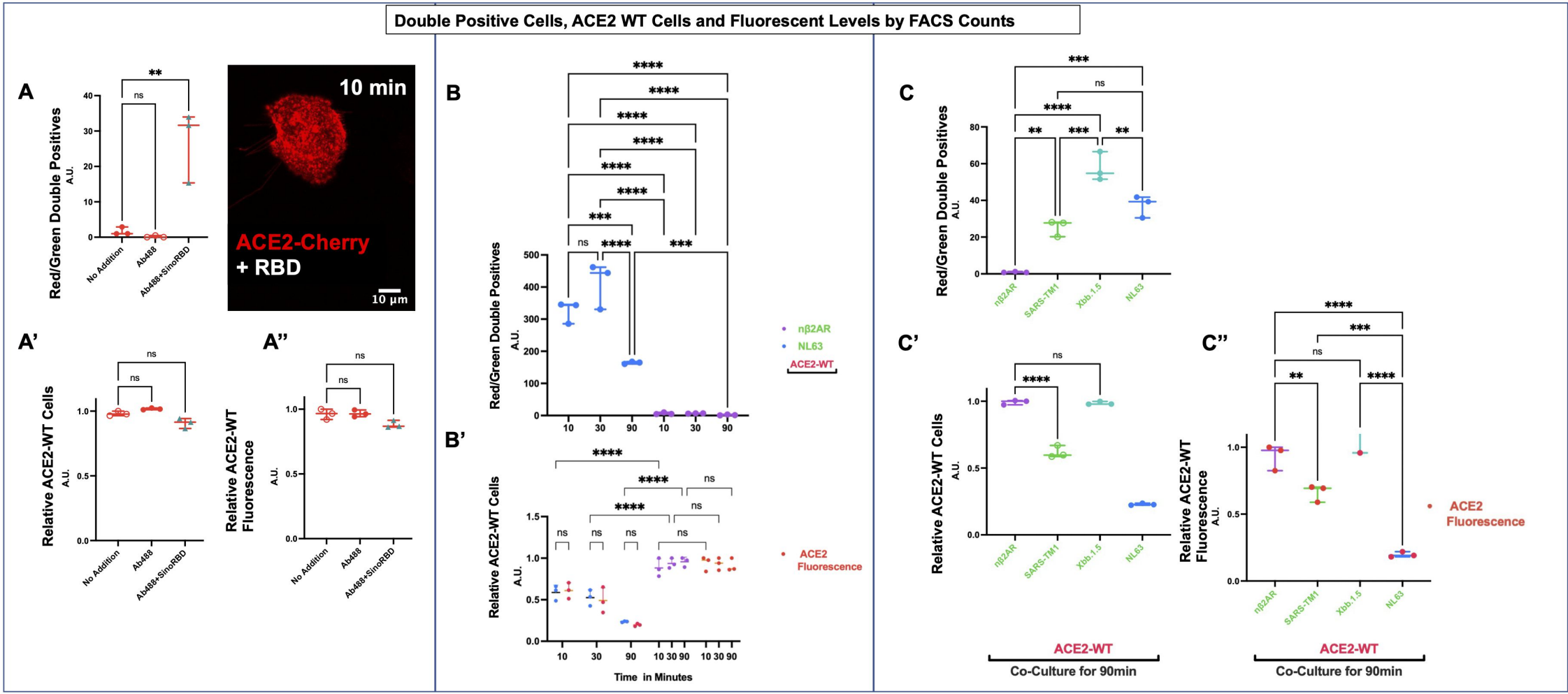

Figure S4

gapTeal fluorescence not affected by RBD-ACE2 binding

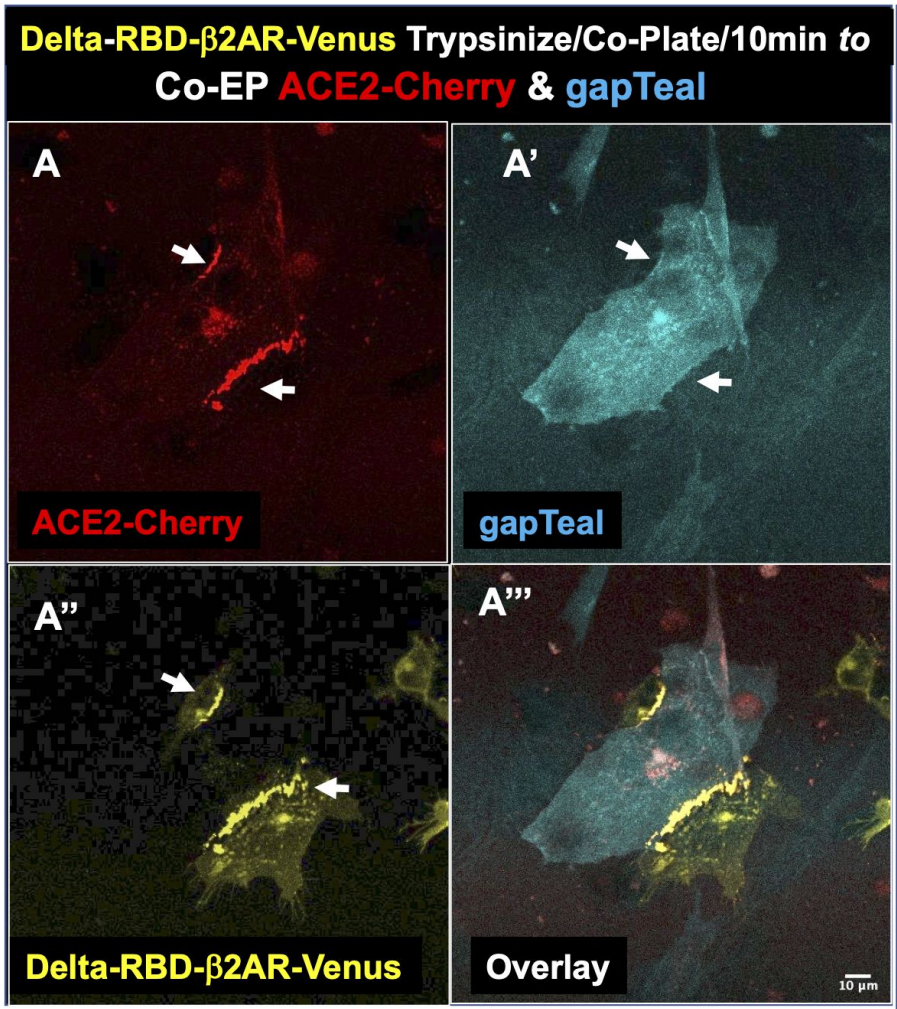

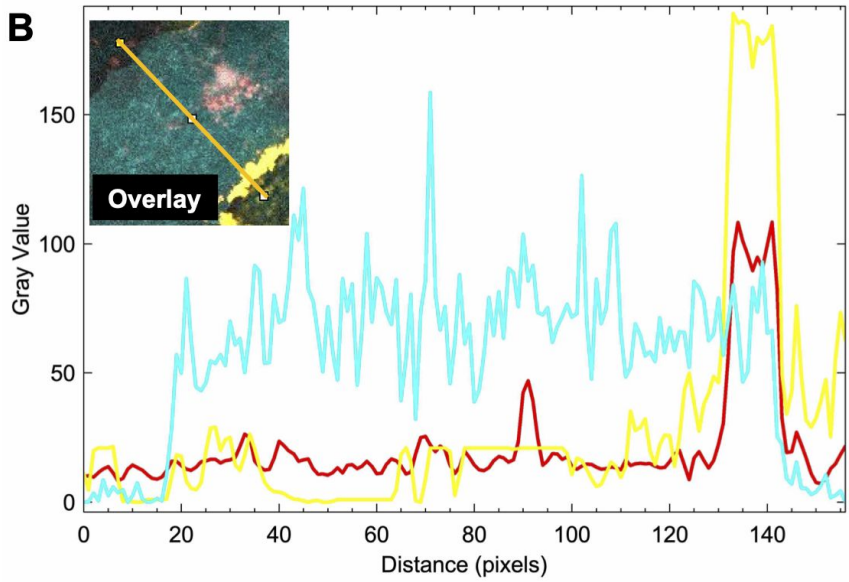

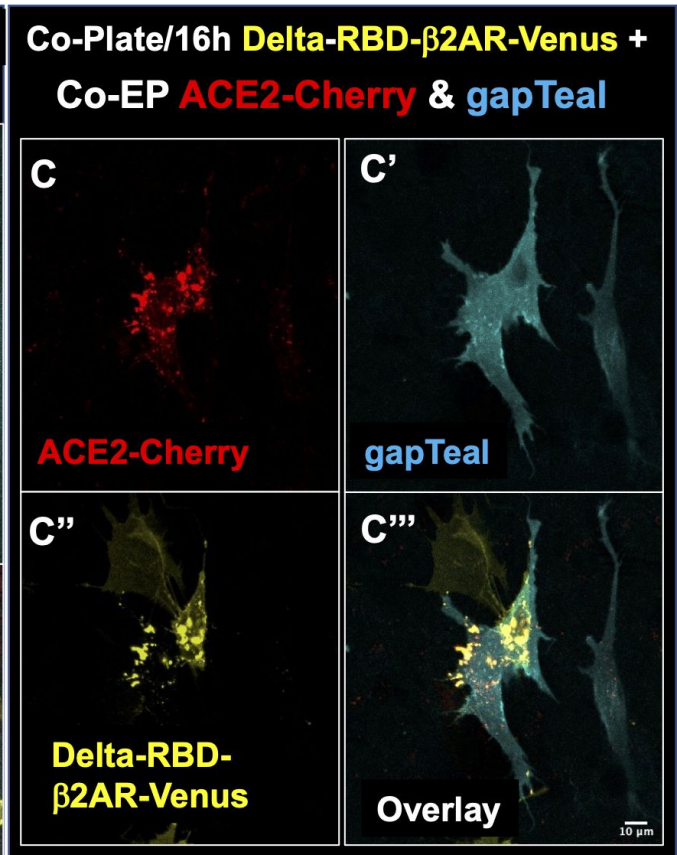

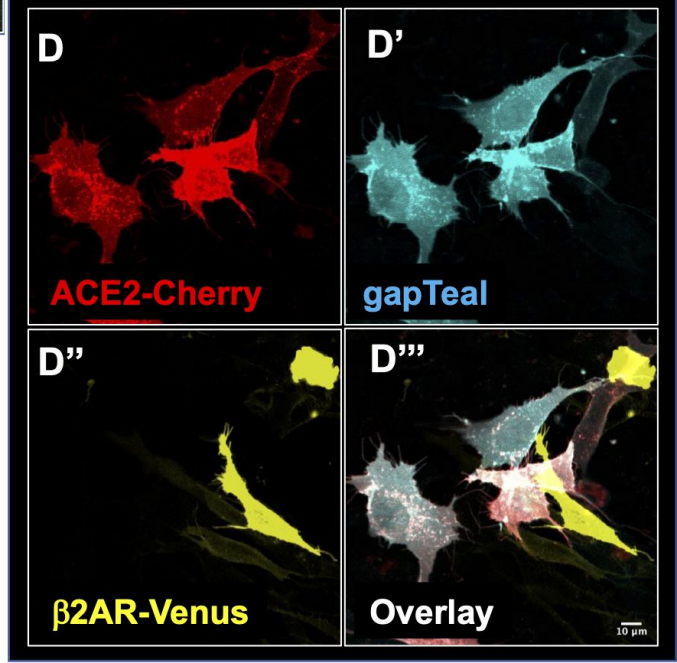

Figure S5

Conservation of Disulfide Loop 4 Residues

11 known β-RBD Cys480-Cys488 Loop 4 and known Kd of RBD-ACE2

1)SARS2	PCNGVEGFNCYFPL	16nM*
2)RaTG13	PCNGQTGLNCYYPL	3.86uM**
3)P5L	PCNGQVGLNCYYPL	no data
4)MP789	PCNGVEGFNCYFPL	no data
5)SARS1	PCT-PPALNCYWPL	58nM*
6)LYRal1	PCT-PPAFNCYWPL	91nM*
7)Rs7327	PCT-PPAFNCYWPL	63nM*
8)Rs4231	SCS-AIGPNCYNPL	69nM*
9a)Rs4084	SCS-AVGPNCYNPL	85nM*
9b)RsSHCO14	SCS-AVGPNCYNPL	29nM*
10)RShSTT200	PCS-VEGPDCYYPL	no data
11)RSYN04	GCN-PSEADCYWPL	15uM^

α-RBD + variant Cys550-Cys577 Loop 3 and known# Kd of RBD-ACE2

1)NL63	C...CFSTVEVPGSCNFPL	35nM#
2)NL63,N578Y	C...CFSTVEVPGSCYFPL	~17nM^^

*Chan et al., 2021;** Liu et al., 2021; ^Zhou et al., 2021

#Wu et al., 2011;^^ Li et al, 2007

Figure S6

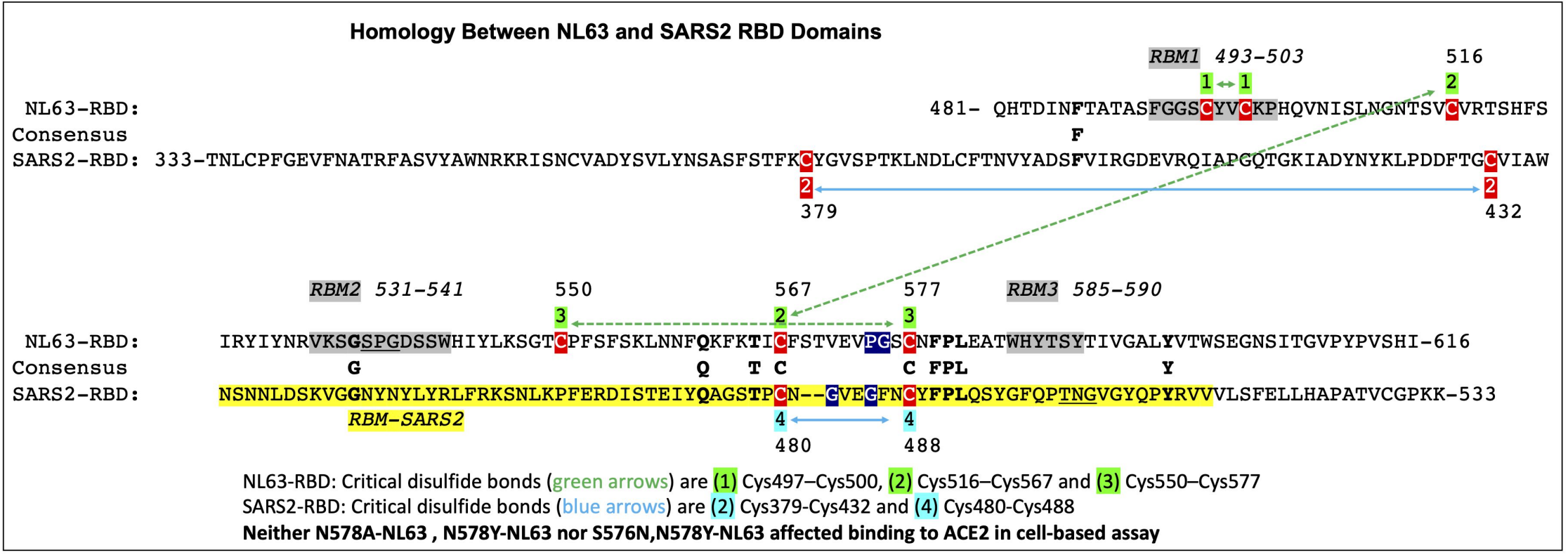
Homology Between NL63 and SARS2 RBD Domains
RBM1 493-503
516
1 1
2
NL63-RBD:
481- QHTDINFTATASFGGSCYVCKPHQVNISLNGNTSVCVRTSHFS
Consensus
F
SARS2-RBD: 333-TNLCPFGEVFNATRFASVYAWNRKRISNCVADYSVLYNSASFSTFKCYGVSPTKLNDLCFTNVYADSFVIRGDEVRQIAPGQTGKIADYNYKLPDDFTGCVIAW
2
2
379
432
RBM2 531-541
550
567
577
RBM3 585-590
3
2
3
NL63-RBD: IRYIYNRVKSGSPGDSSWHIYLKSGTCPFSFSKLNNFQKFKTICFSTVEVPGSCNFPLEATWHYTSYTIVGALYVTWSEGNSITGVPYPVSHI-616
Consensus
G
Q T C
C FPL
Y
SARS2-RBD: NSNNLDSKVGGNYNYLYRLFRKSNLKPFERDISTEIYQAGSTPCN--GVEGFNCYFPLQSYGFQPTNGVGYQPYRVVVLSFELLHAPATVCGPKK-533
RBM-SARS2
4
4
480
488
NL63-RBD: Critical disulfide bonds (green arrows) are (1) Cys497–Cys500, (2) Cys516–Cys567 and (3) Cys550–Cys577
SARS2-RBD: Critical disulfide bonds (blue arrows) are (2) Cys379-Cys432 and (4) Cys480-Cys488
Neither N578A-NL63 , N578Y-NL63 nor S576N,N578Y-NL63 affected binding to ACE2 in cell-based assay

Figure S7

Conservation Between SARS2, RpYN06 and RaTG13

```
                1                         1                   2           3                                   2
SARS2.333.TNLCPFGEVFNATRFASVYAWNRKRISNCVADYSVLYNSASFSTFKCYGVSPTKLNDLCFTNVYADSFVIRGDEVRQIAPGQTGKIADYNYKLPDDFTGCVIAW.436
RpYN06       V   HN       P     E TK  D I   T F   T           S  I     S    T L  FS    V      V
RaTG13                  T                         T                             T
Residues   △456789△123456789△123456789△123456789△123456789△123456789△123456789△123456789△123456789△123456789△12345△
          333    340       350       360       370       380       390       400       410       420       430   436

                                                      4       4                                   3
SARS2.437.NSNNLDSKVGGNYNYLYRLFRKSNLKPFERDISTEIYQAGSTPCNGVEGFNCYFPLQSYGFQPTNGVGYQPYRVVVLSFELLHAPATVCGPKK.529
RpYN06      TAKQ --  ---  F  SH STK       L SDE--------   R------T ST D N NVPLE  AT          N         L
RaTG13       KHI A E   F         A                  K    QT L   Y  YR   Y  D   H             N
Residues   △89△123456789△123456789△123456789△123456789△123456789△123456789△123456789△123456789△12345678△
          437 440       450       460       470       480       490       500       510       520      529
```

RpYN06 Protein homology:

82% overall identity in Spike protein, gaps in Loop4 and Furin Cleavage site.
82% identity to SARS2 outside of 75 residue RBM with all Cysteines conserved.
36% identity to SARS2 inside of RBM with 3 gaps. Two of the gaps cover disulfide Loop4 and delete both cysteines including NCY motif.

Figure S8

Variant/Mutant RBDs and ACE2 *DPF assay*

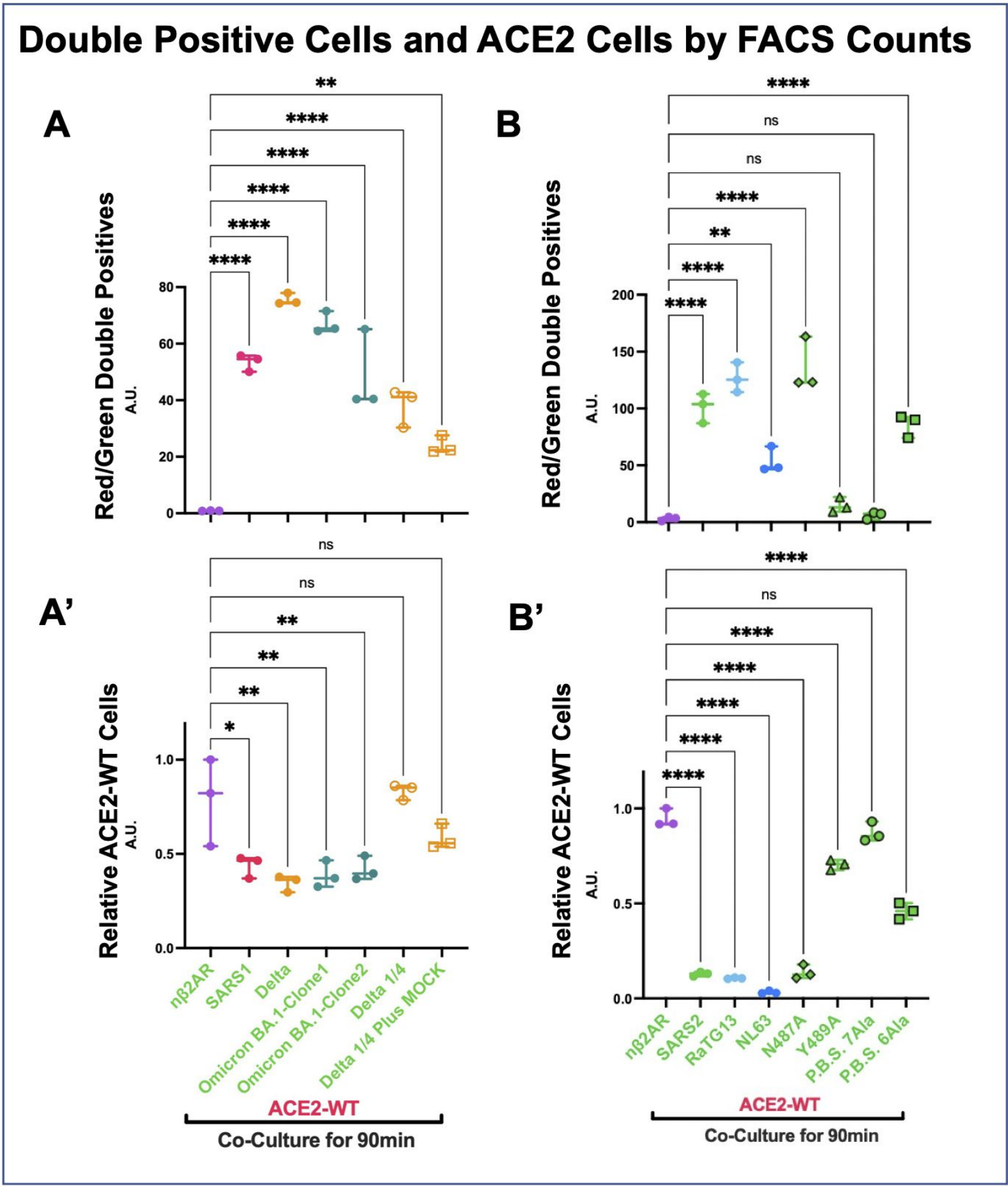

Figure S9

Hi-Magnification Visualization of SARS2-RBD Mutants in Cell-Based Assay

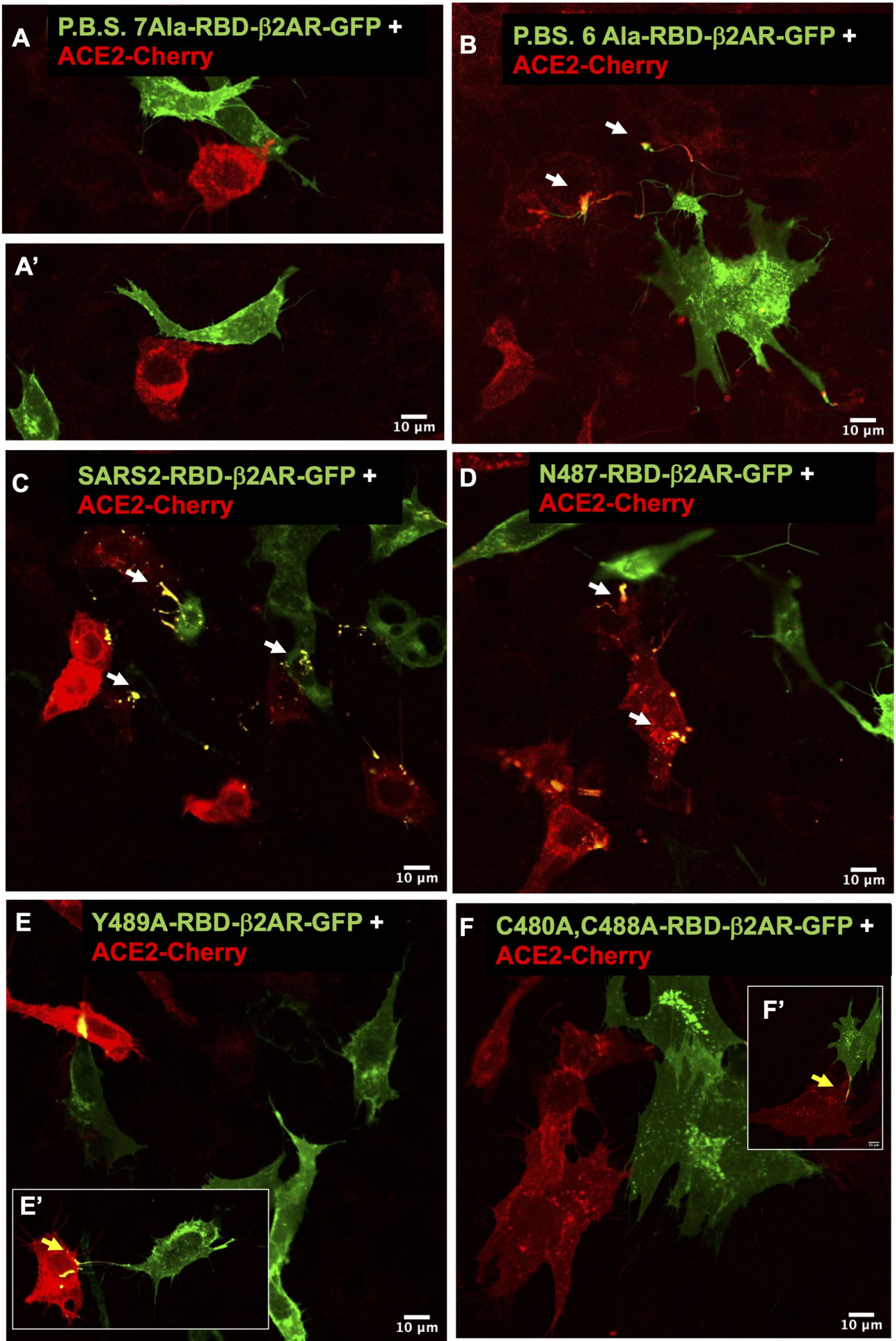

Figure S10
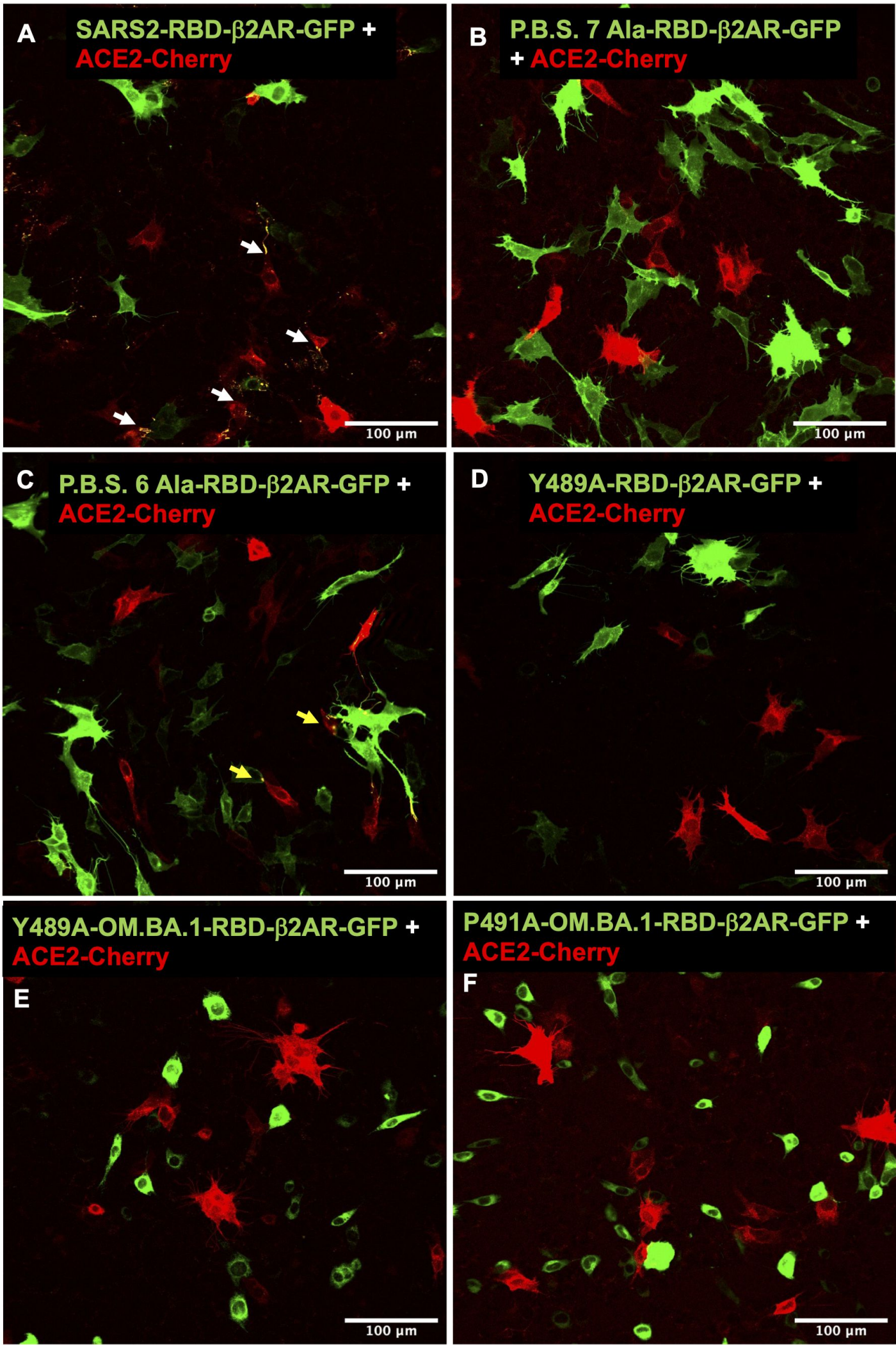
Low-Magnification Visualization of SARS2-RBD Mutants in Cell-Based Assay.